



ORIGINAL ARTICLE

Development of nanoformulation for hyperpigmentation disorders: Experimental evaluations, *in vitro* efficacy and *in silico* molecular docking studies



Yasemin Budama-Kilinc^{a,*}, Bahar Gok^b, Serda Kecel-Gunduz^c, Ebru Altuntas^d

^a Faculty of Chemical and Metallurgical Engineering, Department of Bioengineering, Yildiz Technical University, 34220 Istanbul, Turkey

^b Graduate School of Natural and Applied Science, Yildiz Technical University, 34220 Istanbul, Turkey

^c Faculty of Science, Department of Physics, Istanbul University, 34134 Istanbul, Turkey

^d Faculty of Pharmacy, Department of Pharmaceutical Technology, Istanbul University, 34116 Istanbul, Turkey

Received 24 October 2021; accepted 11 October 2022

Available online 19 October 2022

KEYWORDS

Chlorogenic acid;
Nanoemulsion;
Tyrosinase;
Melanogenesis;
Hyperpigmentation;
Molecular docking

Abstract Hyperpigmentation is a crucial dermatological disorder. This study aims to formulate a nanoemulsion formulation containing chlorogenic acid (CA) for hyperpigmentation treatment, to carry out characterization studies, and to investigate its efficacy and safety *in vitro* and *in silico* analysis.

In line with this purpose, CA nanoemulsions (CA-NEs) were developed using the ultrasonic homogenization method. Accelerated stability tests were performed to examine the kinetic and thermodynamic stability of the CA-NEs to ascertain the presence of any stability issues. After the heating-cooling test, appropriate CA-NEs were stored for 60 days in three different stability environments to examine the physicochemical stability and determine the finalized formulation. The toxicity of the finalized CA-NE formulation was evaluated by genotoxicity/mutagenicity and cytotoxicity tests. The tyrosinase and melanogenesis activities of the finalized CA-NE formulation were determined on the Melanoma B16F0 cell line. Finally, the molecular docking method was used to reveal interactions of CA that play an essential role in tyrosinase inhibition. Additionally, the mushroom and human tyrosinase enzymes were used to determine the activity of CA. In addition, the comparison study with the molecular docking method was carried out using kojic acid as a ref-

* Corresponding author.

E-mail addresses: yaseminbudama@gmail.com, budama@yildiz.edu.tr (Y. Budama-Kilinc), bahar.991@hotmail.com (B. Gok), skecel@istanbul.edu.tr (S. Kecel-Gunduz), ebru.altuntas@istanbul.edu.tr (E. Altuntas).

Peer review under responsibility of King Saud University.



erence molecule.

In conclusion, the molecular docking study, pharmacokinetic analyses, and *in vitro* studies showed that F4P1 coded CA-NE formulation might hold promise as an innovative formulation in cosmetic applications such as skin-lightening effects with its high efficacy and safety profile.

© 2022 The Author(s). Published by Elsevier B.V. on behalf of King Saud University. This is an open access article under the CC BY-NC-ND license (<http://creativecommons.org/licenses/by-nc-nd/4.0/>).

1. Introduction

Melanin is a protective pigment in the skin which has a crucial in blocking UV radiation and protecting DNA from the damaging UV rays that potentially cause skin cancer. Despite its protective effects on the skin, melanin also functions in abnormal pigmentation and melanoma processes (Di Petrillo et al., 2016).

Overproduction of melanin causes significant cosmetic discomfort and may cause distress to the affected person, especially in cases of increased pigmentation such as melasma, solar lentigo (age spots) and freckles in the face area (Panzella and Napolitano, 2019). Additionally, some people may develop post-inflammatory hyperpigmentation after chemical peels, laser treatments, or even acne healing (Baumann and Baumann, 2009). In a study of 2000, dermatology patients with darker skin, pigment disorders were found to be the third most widespread dermatological disorder after acne and eczema (Agbai and Taylor, 2015). According to a prospective cohort experiment on the influence of hyperpigmentation on life standard, while 47.3% of patients reported feeling somewhat self-conscious, 21.8% believed that the people around them focused on their skin view. In addition, 32.7% of the respondents notified that they struggle to camouflage pigment defects, and 23.6% informed that their skin view negatively impacted their daily activities (Taylor et al., 2008).

Melanogenesis is a sophisticated process that involves a combination of enzymatic and chemical-catalyzed reactions. Melanogenesis is responsible for the production of melanin stored in tyrosinase-containing melanocytes (de Freitas et al., 2016). Tyrosinase is the key enzyme involved in the first two steps of the melanogenesis process, catalyzing the hydroxylation of L-tyrosine to 3,4-dihydroxyphenylalanine (L-DOPA) and the oxidation of L-DOPA to L-dopaquinone. Because tyrosinase plays a significant role in melanin biosynthesis, its inhibition is a rational approach to preventing melanin accumulation in the skin. Tyrosinase inhibitors are, therefore, a tempting target as a medicinal and cosmetic active agent of pigmentation disorders (Di Petrillo et al., 2016). However, agents currently available to treat hyperpigmentation have some issues, such as toxicity, low stability, poor skin penetration and/or low efficacy (García-Gavín et al., 2010). Hydroquinone, corticosteroids, kojic acid and arbutin are known as traditional depigmentation agents and have various safety problems due to local or systemic side effects such as prolonged exposure, pigmented contact dermatitis, weak enzyme inhibition, despite their high efficacy, skin irritation and exogenous ochronosis in dark-skinned persons (de Freitas et al., 2016).

Many phytoconstituents can inhibit melanin formation more potent and do not display cytotoxicity or mutagenicity on melanocytes (García-Gavín et al., 2010, Curto et al., 1999, Zhu and Gao, 2008, Gandhi et al., 2012). Natural tyrosinase inhibitors can be affordable, mainly thanks to rich natural resources. In addition, they are generally accepted to be free of harmful side effects (Zheng et al., 2008, Souza et al., 2012).

Polyphenols are a class of compounds that have strong antioxidant capacity and are commonly found in plants. Many polyphenolic compounds have effectively inhibited melanogenesis (Zhu and Gao, 2008). CA, an ester of L-quinic acid and caffeic acid, is a well-known antioxidant found in abundance in coffee, sweet potatoes, and apples (Chinnici et al., 2004, Tang and Liu, 2008) It has been reported in various studies that CA has anti-inflammatory and anticancer activities and is also effective in preventing cardiovascular diseases (Jin et al.,

2005, Miceli et al., 2005, Bonita et al., 2007) and lowering blood sugar levels (Bassoli et al., 2008). Like other plant polyphenols, CA has an inhibitory effect on oxidative stress, and has a protective role against oxidative stress-related diseases. Therefore, its application for topical purposes, such as photoprotection against UV-induced skin damage, skin cancer prevention, and skincare may be beneficial (Caddeo et al., 2008, Vayalil et al., 2003). Unlike other plant polyphenols such as resveratrol, quercetin, and genistein, CA is hydrophilic and water-soluble (Kitagawa et al., 2011). For hydrophilic compounds, intercellular lipids in the stratum corneum acts as a barrier to their intradermal and transdermal delivery (Kim et al., 2001). For this reason, it is required to enhance intradermal delivery to apply CA effectively for topical purposes.

Commonly used cosmetic dosage forms have a low affinity to the skin and low penetration efficacy. Therefore, when conventional cosmetics are used as cosmeceuticals, the active ingredient cannot reach the targeted site, the desired effect can not be obtained (Chanchal and Swarnlata, 2008).

Nanotechnology can eradicate the limitations of conventional dosage forms by lowering the size of phytopharmaceuticals to nanoscale and altering the properties such as permeability, water solubility, and surface properties of phytopharmaceuticals (Altuntaş et al., 2019). One of the critical technologies that can lead to innovative product changes in nanotechnology is NEs.

Currently, NEs are gaining importance as an attractive vehicle for the controlled delivery of cosmetics and finalized penetration of either hydrophilic or lipophilic active ingredients in particular skin layers by increasing their concentration in the skin. Another advantage is that the small droplet size with a large surface area allows the active ingredients to be effectively distributed to the skin. NEs are cosmetically acceptable systems since there are no stability problems such as creaming, sedimentation, flocculation or coalescence occurring in microemulsions. Since NEs are non-toxic and non-irritating, they can be safely applied to the skin and mucosa. Unlike microemulsions that usually require high concentrations of surfactant of 20%, w/w and above, NEs can be manufactured using reasonable surfactant concentrations (5–10%, w/w).

Considering the information mentioned earlier, this study aimed for the first time to create a formulation in the NE form, including CA in the therapy of hyperpigmentation via intradermal route. At first, the toxicity of seven different concentrations of CA was examined in the immortalized human keratinocytes (HaCaT) cell line and the highest safe-dose of CA suitable for use in formulations was determined. Then, CA-NE formulations were manufactured using by ultrasonication technique. To determine the durability of the formulations, the samples were subjected to accelerated stability studies and the physicochemical properties were also investigated under different storage conditions for 60 days. Furthermore, the *in vitro* release analysis of the finalized NE formulation was performed by the dialysis membrane technique, and the *in vitro* mutagenicity and cytotoxicity of CA-NE formulation were evaluated by Ames/Salmonella and MTT tests, respectively. Besides, the effect of the CA-NE formulation on cell viability was investigated on the HaCaT cell line, and the activity of CA-NE formulation on tyrosinase enzyme and melanogenesis process was also examined on the Melanoma B16F0 cell line. Finally, molecular docking studies were performed to evaluate the tyrosinase inhibitory activity of CA in comparison with kojic acid, which is considered a model molecule.

2. Materials and methods

2.1. Materials

CA was purchased from Alfa Aesar. Pluronic® F-68 (HLB value: 29), DL-alpha tocopherol acetate, MgSO₄·7H₂O, C₆H₈O₇·H₂O, K₂HPO₄, NaH₂PO₄·H₂O, Na₂HPO₄·2H₂O, -NaOH, NaCl, MgCl₂·6H₂O, KCl, L-histidin, D-biotin, NaH₂NH₄(-PO₄·4H₂O) and 4-nitro-*o*-phenylenediamine (NPD) were purchased from Sigma-Aldrich. Ethanol (≥99.5%) was obtained from Tedia. Undecyl alcohol (Sensiva® PA 30) was purchased from Schülke. Agar was purchased from Difco. Nutrient broth was purchased from Oxoid. Mueller-Hinton broth (Oxoid) and Mueller Hinton agar were purchased from Sigma-Aldrich. Isodecyl neopentanoate (DUB™ VCI 10) was supplied from Stearinerie Dubois. Caprylic/capric Triglyceride (Labrafac™ Lipophile WL 1349) Transcutol® HP (HLB value: 4.2) and oleoyl polyoxyl-6 glyceride (Labrafil® M 1944 CS) were purchased from Gattefosse. Sodium azide (NaN₃) was purchased from Merck. Immortalized human keratinocytes (HaCaT) cell line was provided from ThermoFisher Scientific, and melanoma B16-F0 (ATCC® CRL-6322™) cell line was purchased from the American Type Culture Collection. L-Dopa, Dulbecco's Modified Eagle Medium (DMEM), dimethyl sulfoxide (DMSO), 3-(4,5-dimethyl-2-thiazolyl)-2,5-diphenyl-2H-tetrazolium bromide (MTT), ethylenediamine tetraacetic acid (EDTA), and trypan blue (0.4%, liquid) were purchased from Sigma-Aldrich. Penicillin-streptomycin, fetal bovine serum (FBS), and trypsin/EDTA (0.25%/2.21 mM) were acquired from Gibco.

2.2. Methods

2.2.1. Fabrication of CA-NEs

Sixteen different CA-NEs were prepared by ultrasonic homogenization method (Liao et al., 2022). Different homogenization conditions such as with/without pre-emulsification stage before ultrasonication process with different ultrasonication time were used in order to obtain the optimum formulation. All NEs were prepared with different ratios of oil phase to the S_{mix} (surfactant and cosurfactants mixture) (1:1.5, 1:2, 1:4, 1:5). Pluronic F® 68 as a surfactant and Transcutol® HP and Labrafil® M 1944 CS as co-surfactants were used in order to obtain the optimum formulation. The coarse emulsion was obtained with pre-emulsification method by using a rotor-stator type homogenizer for 5 min at 8100 rpm. Then, the coarse emulsion was exposed to the ultrasonication (20 kHz at 750 W maximum power output) (Diane and Burgess, 2014). Sonotrode was used containing a piezoelectric crystal (time: 15 and 30 min; amplitude: %50 with 30 s pulse on and 30 s pulse off). Finally, characterization studies were applied on the prepared NEs and then the various stability tests were carried out.

2.2.2. Characterization of CA-NEs

2.2.2.1. Photon correlation spectroscopy analysis of CA-NEs. Average droplet diameter and polydispersity index values of the CA-NEs were acquired by photon correlation spectroscopy (Malvern Instruments, UK) (Khalil et al., 2021). Zeta potential was measured using the same device through laser Doppler anemometry which analyzes speed and direction. Samples

diluted 1:100 in distilled water were analyzed within 24 h. Light scattering was monitored with a zeta DTS1060C cell at 25 °C at a 90° angle. All measurements were performed in triplicate.

2.2.2.2. pH and conductivity analysis of CA-NEs. To evaluate the stability of emulsions, it is crucial to monitor pH throughout stability studies since variations in pH values suggest that chemical processes are taking place that may degrade the final product's quality (Bernardi et al., 2011). Electrical conductivity measurement is a valuable tool to identify the type of emulsion and track changes during manufacture or storage (Ozkan et al., 2022). The pH and conductivity of the CA-NEs were made using a pH meter (Ohaus® Starter 3100M). Measurements were made in triplicate at 25 °C.

2.2.2.3. Viscosity analysis. Viscosity analysis is a popular technique for assessing a nanoemulsion's stability under stressful circumstances (Romes et al., 2021). Viscosity analysis was performed using a Brookfield cone-plate viscometer (HA DV3T Rheometer) by measuring the viscosity values of the CA-NEs samples at different shear rates (Rajitha et al., 2019).

2.2.2.4. Active ingredient content analysis. Active content analysis is used to evaluate the stability of drugs in any pharmaceutical formulation. In this experiment, each three batches (250 µL) of the finalized CA-NE formulation were dissolved in 10 mL ethanol and sonicated in an ultrasonic bath for 30 min (Ozkan et al., 2022). Subsequently, CA content in sample was determined using the curve equation spectrophotometric analysis of CA.

2.2.2.5. The morphology analysis. The morphology of the CA-NEs was investigated with the transmission electron microscope (TEM) (JEOL TEM 1400 Plus) (Ghazy et al., 2021). The appropriate amount of the formulation was placed on a carbon-coated grid, and images were viewed under a voltage of 80 kV.

2.2.3. Accelerated stability studies

Thermodynamic stability and heating-cooling cycle tests were performed as in our previous work (Ozkan et al., 2022).

2.2.4. Physicochemical stability studies

The CA-NEs without any stability problems detected in the accelerated stability tests were subjected to physicochemical stability studies (Kildaci et al., 2021). Freshly prepared CA-NEs were stored in closed glass vials in three different conditions to examine the physicochemical stability. Characterization of the formulations was observed concerning their average droplet size, PdI, zeta potential, pH, electrical conductivity, and viscosity on predetermined days (1st, 7th, 30th, and 60th days).

2.2.5. The calibration curve of CA

The calibration curve of CA was performed using a UV-vis Spectrophotometer (Shimadzu, Japan). The maximum absorbance values were obtained at 324 nm for seven different concentrations of CA in ethanol, and the calibration curve of CA was plotted (Hosseini et al., 2013). The curve equation was used to determine the amount of CA in the active ingredient

content analysis, physicochemical stability tests, and *in vitro* release study.

2.2.6. *In vitro* release study of CA-NEs

In vitro release study was exerted on the optimum formulation selected based on all stability tests. 1 mL of the CA-NEs was placed in a dialysis capsule in triplicate. 50 mL of phosphate buffer solution (PBS) pH 5.5; Ethanol (60:40 v/v) was used as the release media (Hosseini et al., 2013). The incubation process of the samples was performed in the shaking water bath at 32 °C (Azarmi et al., 2007) at 120 rpm (Budama-Kilinc et al., 2020, Egil et al., 2020). At certain time intervals, 1 mL of release medium was withdrawn, and 1 mL of fresh buffer solution was added to the release medium. The amount of CA released from samples was by a UV-vis spectrometer.

2.2.7. AMES/Salmonella test

The mutagenic properties of the samples were evaluated by AMES/Salmonella test using TA98 and TA100 strains of *S. typhimurium* (Maron and Ames, 1983, Hergueta-Castillo et al., 2022, Guzelmeric et al., 2022, Ibarra-Berumen et al., 2022). Concentrations were chosen as 0.25, 0.5 and 1 mg/plate for the blank NEs and CA-NEs. The concentrations (0.045, 0.09, 0.18 mg/plate) of CA were used according to the amount contained in CA-NEs. NPD and NaN₃ were employed as the positive control; ultrapure water was used as the negative control. Samples with different concentrations were incubated with bacteria at 37 °C for 48 h. After incubation, the mutagenicity of blank NEs, CA-NEs and CA was evaluated compared to the negative control.

2.2.8. *In vitro* cell culture studies

HaCaT and Melanoma B16-F0 cell lines were cultured in DMEM medium supplemented with 10% FBS and 1% penicillin-streptomycin and incubated at 37 °C in an incubator containing 5% CO₂.

2.2.8.1. Cytotoxicity analysis. HaCaT cells were used to evaluate the cell viability of CA and the finalized CA-NE formulation (Pacheco et al., 2019). The cells were seeded at a density of 5×10^3 cells/well and treated in six replicates for 24 h with seven different CA concentrations (ranging from 22.5 to 1440 µg/mL) after 24 h of incubation. After incubation, MTT (0.5 mg/mL) was added and incubated for 4 h. DMSO (100 µL) was then added to the wells, and the plates were measured using an ELISA reader at 570 nm. The cytotoxicity of CA was evaluated by comparison with the untreated control group. The cell viability (%) was calculated using Eq. (1).

$$\text{Viability \%} = \frac{\text{Absorbance of Experimental Group}}{\text{Absorbance of Control Group}} \times 100 \quad (1)$$

2.2.8.2. Tyrosinase and melanogenesis activity. Tyrosinase and melanogenesis activity of the finalized CA-NE formulation were performed as in our previous work (Ozkan et al., 2022). Three different concentrations of the finalized CA-NE (0.25, 0.5 and 1 mg/mL) were used in the study.

2.2.9. Molecular docking study and ADME analysis

An established approach to treating hyperpigmentation is tyrosinase inhibition, so there is a need to reveal interaction sites of CA with tyrosinase. In terms of its molecular structure, CA belongs to a group of polyphenol ester families including hydroxycinnamic acids. Cinnamic acid and benzoic acid analogues having a phenyl ring have been found to exhibit tyrosinase inhibitory activity. Cinnamamide derivatives also have a much higher inhibitory effect on mushroom tyrosinase and melanin production than specific tyrosinase inhibitor (Ullah et al., 2018, Shi et al., 2005, Menezes et al., 2011, Milovsky et al., 2013). In this study, we pay attention to molecular docking analysis to find the binding position of CA and kojic acid with having anti-tyrosinase properties to the mushroom tyrosinase and human tyrosinase enzymes. In order to reveal the tyrosinase inhibitory role of CA and kojic acid, which binds to the active site of tyrosinase, docking analysis was performed using Schrödinger Maestro program (Schrodinger, 2019, Friesner et al., 2004, Halgren et al., 2004). The structure of *Agaricus bisporus* Mushroom Tyrosinase with 2.78 Å resolution crystal structure (PDB ID: 2Y9X) and the human tyrosinase related protein 1 (PDB ID: 5M8L) were preferred as possible receptors for docking calculations (Ismaya et al., 2011, Lai et al., 2017) and obtained by loading PDB file from RCSB Protein Data Bank (PDB) web sites (Ismaya et al., 2011, Lai et al., 2017). The edited deficient crystal data of the down-loaded proteins were provided using the Swiss Model server (Bienert et al., 2017). The Glide SP module of Maestro version 11.4, the Schrodinger Software, was employed for molecular docking and ADME calculations. The initial molecular structure of CA and kojic acid, known for its antibacterial and anti-fungal properties as well as its anti-tyrosinase properties, were uploaded from CheBI (Hastings et al., 2016) and ChemSpider (CSID:3708, 2022) systems with ID: 16112 and 3708, respectively. They were built and finalized using Gaussian software (Frisch et al., 2010) with DFT B3LYP/6-311++g(d,p) basis set. To generate all possible stereoisomers of CA and kojic acid the finalized molecular structures selected as the ligands, the OPLS force field (Harder et al., 2016) was used. By deleting structures other than the A chain (B, C and D chains, all waters, etc.) in the structure and adding polar hydrogens to heavy atoms, bond orders were assigned, and defective residues in the receptor were identified and analysed by preprocessing. Charges were also determined using PROPKA (Sondergaard et al., 2011) at pH 7.0. After optimization, the energy minimization for the receptor was carried out using 0.3 Å RMSD and OPLS3 force field (Sastry et al., 2013). After determining a cubic box-shaped grid of a certain size centered on the gravity of the ligand and determining the rotatable residues in the binding region of the receptor, in particular the thiol and hydroxyl group-containing residues, docking analysis was performed. Using Qik-Prop module (Schrödinger, 2020) of the software preferred to define the pharmacokinetic and physicochemical properties for CA and kojic acid based on the results of the docking analysis with mushroom tyrosinase receptor. The properties such as molecular weight (M_w), human oral absorption percentage, estimated octanol/water partition coefficient (QPlogPo/w), polar surface area (PSA) and Lipinski's five-rule conformity were also calculated and evaluated.

2.2.10. Statistical analysis

In the study, statistical analysis of cytotoxicity, melanin inhibition, anti-tyrosinase activity, and mutagenicity test results were determined using ANOVA included in the IBM SPSS Statistics 22 package program. The Tukey test at $p < 0.05$ determined the significance level of the differences between the control and treatment groups. In addition, the mutagenicity test result was evaluated according to [Mortelmans and Zeiger \(2000b\)](#).

3. Results and discussion

3.1. Assessment of cell viability of CA

Melanogenesis is a complex process involving the enzyme tyrosinase, and there are studies examining the effect of CA on tyrosinase and melanogenesis activity in the literature. However, there is not any nano-sized formulation of CA in nanoemulsion dosage form that has been studied so far ([de Freitas et al., 2016](#), [Li et al., 2014](#)). In our study, at first, the cell viability study was performed for seven concentrations of CA ranging between 1440 and 22.5 $\mu\text{g/mL}$, to determine the maximum concentration of CA could be used in nanoemulsion production process. According to ISO 10993-5, the cell viability percentages above 80% are non-cytotoxicity; weak between 80–60%; 60–40% is considered moderate and below 40% strong cytotoxicity ([10993-5, 2009](#)). MTT assay was performed to determine the cell viability of CA in the HaCaT cell line. As seen in [Fig. 1](#), it was observed that the % cell viability decreased as the concentration of CA increased compared to the control group; however, there was no statistically significant difference ($p > 0.05$). Li et al. reported that the 354 $\mu\text{g/mL}$ concentration of CA had no toxicity and reduced tyrosinase activity in their study examining the CA effects on Melanoma B16 cells ([Li et al., 2014](#)). According to the results, it was decided to use 180 $\mu\text{g/mL}$ CA concentration with cell viability of 81.62% in nanoemulsion formulation production studies.

3.2. Preparation and characterization of CA-NEs

Human skin contains melanin, which primarily serves as a photoprotective mechanism. However, excessive melanin production or aberrant melanin distribution can lead to uneven skin hyperpigmentation. Hyperpigmentation may result from exposure to specific drugs and chemicals and certain medical diseases like melasma and age spots ([Chang, 2012](#)). According to current studies, many melanogenesis abnormalities have also been connected to neurodegenerative illnesses, including Parkinson's and Alzheimer's ([Youdim, 2006](#)). Therefore, there is a great demand for developing new drugs to prevent hyperpigmentation disorders.

In our study, it was developed a new NE formulation containing CA to reduce skin pigmentation and investigate its inhibitory activity on tyrosinase enzyme and melanogenesis in B16F0 melanoma cells. NEs containing CA were successfully manufactured using the ultrasonication method. NEs prepared in preliminary studies were evaluated regarding their photon correlation spectroscopy analysis. The identified formulations were then subjected to accelerated stability tests. Results showed that the average droplet size, PDI, and zeta potential of all prepared NEs were varied from 57.16 ± 0.86 nm to 132.46 ± 2.70 nm, 0.128 ± 0.07 to 0.255 ± 0.00 and -4.67 ± 1.29 mV to -22.96 ± 7.28 mV, respectively. All the prepared CA-NEs seemed low viscosity, bluish and milky. The identified formulations were then subjected to accelerated stability tests. The smallest mean droplet size (57.16 ± 0.86 nm) was obtained with the NE formulation containing an oil phase/ S_{mix} ratio of 1:5. On the other hand, the NE formulation developed with an oil phase/ S_{mix} ratio of 1:2 had the largest droplet size (132.46 ± 2.70 nm). Similar results were also obtained by [Sarheed et al. \(2020\)](#) ([Sarheed et al., 2020](#)). They found that at lower oil concentrations, droplet sizes decreased significantly with an increase in surfactant concentration (a low oil-to-surfactant ratio).

It has been reported in the literature that NEs with an average droplet size of 100–200 nm are more suitable for penetration ([Sabouri et al., 2018](#), [Ngan et al., 2014](#)). Therefore,

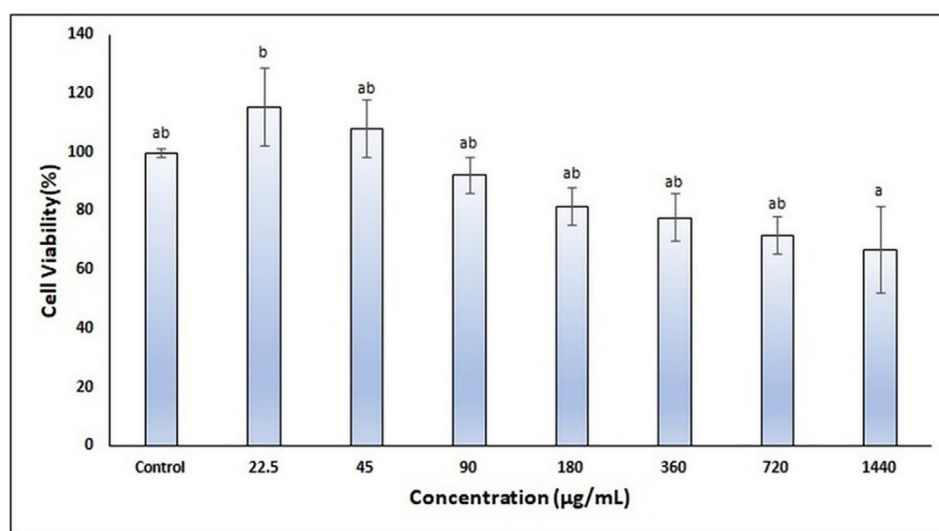


Fig. 1 Cell viability results of CA in the HaCaT cell line.

considering the particle size, the NEs prepared in our study are thought to be convenient for topical applications.

PdI value has been used to analyze the homogeneity of the droplets in the NEs. A PdI value close to zero indicates a monodisperse system, while a PdI value close to one indicates a polydisperse system with heterogeneous droplet sizes (Tang et al., 2012). Pongsumpun et al. underlined that a NE formulation with a PdI value of <0.3 is considered a monodisperse system (Pongsumpun et al., 2020). In our study, all NEs were monodispersed and homogeneous, since their PdI value is lower than 0.3.

Generally, a zeta potential value exceeding ± 30 mV is ideal for preventing aggregation in colloidal systems that are electrostatically stable due to electrostatic forces such as emulsions droplets (Wik et al., 2020). However, the relatively low zeta potential value (ranging from -4.67 to -22.96 mV) of the prepared CA-NEs may be due to the presence of NEs, the Pluronic PEO block copolymer located on the surface of the oil droplets.

Generally, preparation of coarse emulsion prior to ultrasonication process is recommended to improve the sonication process (Abbas et al., 2013). In our study, it was investigated whether coarse emulsion preparation had an effect on particle size and PdI before ultrasonication. As a result, we found that pre-emulsification had a negligible role on the droplet size and PdI of CA-NEs. The particle size and PdI values of the F4P1 coded NE, which were prepared without the pre-emulsification step of the F4 series selected for physicochemical stability studies, were found to be particle size 106.93 ± 1.25 , 0.128 ± 0.07 , respectively. The F4P3 coded NE and PdI values, which had the same composition but were prepared with the pre-emulsification step, were found to be 106.56 ± 1.55 and 0.148 ± 0.02 , respectively (Table 1). Our study is similar to the one reported that the pre-emulsification step of linseed oil-loaded NEs had a negligible effect on droplet size. (Kentish et al., 2008). In similar fashion, Takegami et al. used the ultrasonication technique to formulate a NE formulation containing a tiny average droplet diameter (50 nm) without a pre-emulsification step (Takegami et al., 2008).

Ultrasonication time might have a significant role on droplet size and PdI. (Abbas et al., 2013). To understand the effect of the duration of the ultrasonication process on the particle size and PdI of our NEs, we tried two different sonication times, 15 or 30 min. Consequently, a slight raise in particle size and a negligible effect on PdI were observed due to extending the ultrasonication process from 15 min to 30 min. In the F4 series, the particle size and PdI values of F4P1, which was ultrasonicated for 15 min, were 106.93 ± 1.25 and 0.128 ± 0.07 , respectively, while the particle size and PdI values of F4P2, which was ultrasonicated for 30 min, were 118.23 ± 2.28 and 0.179 ± 0.01 , respectively (Table 1). In line with our results,

Guedes Silva and Kawazoe Sato reported that increasing sonication time (from 5 min to 10 min or 10 min to 15 min) resulted in emulsions with larger droplet size (Silva and Sato, 2019). This situation can be explained by a higher probability of droplet collisions resulting in coalescence because of over-processing (Mahdi Jafari et al., 2006).

Our skin has an acidic pH of 4.0–6.0 (Ali and Yosipovitch, 2013) and often a pH in the range of 4.0–7.0 is suitable for topical application (Roselan et al., 2020). The pH values of our formulations were demonstrated to be compatible with the physiological skin pH (Table 1).

Conductivity is defined as the solution's ability to conduct electricity flow and is related to the amount of all ions present in the solution. This parameter can help to determine the type of NEs produced (Jiang et al., 2013). In our study, high conductivity measurements showed that the external phase of CA-NEs is water, suggesting that the NEs formed are oil in water-type NEs (O/W) (F4 series: minimum $75.70 \mu\text{s}/\text{cm}$; maximum $95.53 \mu\text{s}/\text{cm}$) (Table 1). O/W type emulsions are more favorable as they leave a less greasy feel once applied to the skin (Roselan et al., 2020).

The fluidity with relative physical stability provides a pleasant physical characteristic and good sensorial skin feel (even in the absence of a thickening agent) that allows the use of NEs in liquid cosmetic products (lotions or transparent milk) (Tadros et al., 2004, Bugaj, 2015). NEs can flow easily over the skin without creaming and shiny appearance after the topical application (Sonneville-Aubrun et al., 2004). In our study, as the oil concentration was increased by maintaining the S_{mix} concentration constant, an increasing trend in viscosity of the NEs was observed. The viscosity values of the NEs manufactured without pre-emulsification with 15 min ultrasonication procedure, were 66.30, 27.10, 21.10 and 19.50 cP at 70 rpm for 1:1.5, 1:2, 1:4 and 1:5 oil phase to the S_{mix} ratio of CA-NEs, respectively. This result can be attributed to the data that in emulsions containing higher oil phase concentrations, the droplets are packed more densely, which increases the emulsion viscosity (Dickinson and Golding, 1997), increases the interactions between droplets and network formation (Nikovska, 2012), and thus reduces the creaming rate. For all CA-NEs, there was not a substantial change in the viscosity of the NEs when rotation speed was increased, which indicated the Newtonian flow behavior of NEs. These results are in line with literature findings (Shakeel et al., 2009).

3.3. Accelerated stability studies

NEs are thermodynamically unstable colloidal dispersions; therefore, stability problems such as creaming or phase separation on long-term storage are likely to occur (Wik et al., 2020).

Table 1 Characterization results of CA-NEs belonging to F4 series selected for physicochemical stability studies (means \pm SD, n = 3).

| Code | Droplet Size (nm) | PdI | Zeta Potential (mV) | pH | Conductivity ($\mu\text{s}/\text{cm}$) | Organoleptic characteristics |
|------|-------------------|------------------|---------------------|----------------|--|------------------------------|
| F4P1 | 106.93 ± 1.25 | 0.128 ± 0.07 | -13.29 ± 9.98 | 4.55 ± 0.1 | 78.10 ± 2.34 | Milky and bluish aspect |
| F4P2 | 118.23 ± 2.28 | 0.179 ± 0.01 | -9.54 ± 1.15 | 4.43 ± 0.2 | 95.53 ± 1.60 | Milky and bluish aspect |
| F4P3 | 106.56 ± 1.55 | 0.148 ± 0.02 | -9.38 ± 0.41 | 4.57 ± 0.1 | 82.25 ± 0.07 | Milky and bluish aspect |
| F4P4 | 119.46 ± 1.42 | 0.215 ± 0.02 | -4.67 ± 1.29 | 4.48 ± 0.3 | 75.70 ± 0.26 | Milky and bluish aspect |

Therefore, stress tests (centrifugation and thermal stability) were performed on the CA-NEs to accelerate the emulsion breakdown. No physical stability problems such as precipitation, phase separation, or creaming were observed after the stress tests. Therefore, all NEs successfully passed the accelerated stability tests and were exposed to the heating-cooling test. Temperature is also one of the most critical factors contributing to instability. This effect can usually occur when the formulation is stored at low (for example, 5 °C or below) or high temperatures (for example, 40 °C or above). Therefore, a heating-cooling cycle test was conducted for six cycles to evaluate the effects of extreme temperature changes on the stability of the selected CA-NEs. At the end of this test, it was detected that all the tested NEs remained in a homogeneous milky bluish form without any visually observed stability issues.

Considering the data on the heat-cooling cycle test results regarding the average droplet size of the F4 series formulations, it was determined a slight increase in average droplet size (Table 2). However, all formulations still remained at desired droplet sizes, between 20 and 200 nm, at the end of six cycles. The PdI values of the CA-NEs were below 0.2, with a decrease at the end of the test, indicating a uniform droplet size distribution even under vigorous environments. Our results regarding the decrease in PdI values after six cycles are in line with the results of the NEs containing *Ocimum sanctum* Linn ethanolic extract developed by Chaiyana et al. In their study; they noticed a decrease in PdI value of their NEs After completing the eight cycles of heating-cooling (24 h each at 4 °C and 45 °C) (Chaiyana et al., 2020). Zeta potential of the finalized NE formulation (F4P1) decreased from -13.29 ± 9.98 mV to -35.0 ± 7.68 mV, suggesting the satisfactory droplet charge to stabilize the NE formulation (Table 2).

3.4. Physicochemical stability studies

A decrease in active constituent content (chemical instability) or a physical instability may be seen due to manufacturing processes, formulation excipients, and environmental conditions such as heat, moisture, or light. Therefore, stability studies on selected CA-NEs series (F4) were performed by keeping the samples in three different stability test environments for two months. Organoleptic control, the average droplet size, PdI, zeta potential, pH, conductivity, viscosity, and drug content analysis were conducted during storage time period.

When organoleptic control was performed in all NEs, they were determined to be durable without any physical stability

problems. However, higher increases were observed as the storage temperature increased, although the droplet size was still in the nano-size range during the test period (Table 3). These findings come in good agreement with results of previous studies that used the NE technology associated with the increase in droplet diameters throughout stability period (Kildaci et al., 2021, Karthik and Anandharamakrishnan, 2016, Arbain et al., 2018). An increase in average droplet diameter can be caused by increased in storage temperature, causing droplet aggregation. The droplet size increase was determined to be slower for the samples kept at 5 ± 3 °C than those kept at high temperatures.

It was purported that when emulsions are kept at a lower temperature, the molecular motion will decline accordingly (Karthik and Anandharamakrishnan, 2016). It was reported by Adjonu et al. that the emulsion kept at a higher temperature showed multimodal size distribution compared to the emulsion held at lower temperature (Adjonu et al., 2014). Based on this information, it might be suggested that a lower storage condition of 5 ± 3 °C would be appropriate for storing CA loaded NE formulations.

In this study, NEs of the F4 series have low PdI values (below 0.3) during the test period of 60 days, indicating superior stability of the system. The finalized CA-NEs had PdI values in the range of 0.050–0.139 over 60 days (Table 3). This result demonstrates the adequate formulation composition of the prepared NEs and convenient method of manufacture to develop a stable NE formulation with a homogenous droplet size distribution.

The zeta potential of the finalized CA-NEs varied over 60 days at varied conditions, varying from -8.8 to -16.7 mV (Table 3). There was no significant change in the zeta potential value of the F4P1 stored in the refrigerator on day 60th (-15.0 mV) compared to the zeta potential value belonging to the first day (-13.3 mV).

It may be useful to test the pH profiles of formulations kept under specific conditions to understand the chemical stability performance. If it is determined that the pH values measured at various time points are in the skin pH range, it can be purported that the formulations can be used safely on human skin (Muhammad et al., 2014). In this study, it can be clearly observed that the change in the pH of the F4 series NEs was insignificant for different time points at different storage conditions, and they were found to be suitable for topical application (Table 3).

High conductivity is obtained with an oil in water-type NEs, and the phase inversion depending on the destabilization, can lead the conductivity differences in NEs over time (Kildaci

Table 2 Comparison of CA-NEs belonging to F4 series before and after the heating-cooling test (H-C Test: Heating-Cooling Test) (means \pm SD. n = 3).

| Formulation Code | Average Droplet Size (nm) | | Polydispersity Index (PdI) | | Zeta Potential (mV) | |
|------------------|---------------------------|------------------|----------------------------|------------------|---------------------|------------------|
| | Day 1 | H-C Test | Day 1 | H-C Test | Day 1 | H-C Test |
| F4P1 | 106.93 \pm 1.25 | 150.6 \pm 2.02 | 0.128 \pm 0.07 | 0.046 \pm 0.37 | -13.29 \pm 9.98 | -35.0 \pm 7.68 |
| F4P2 | 118.23 \pm 2.28 | 160.4 \pm 0.98 | 0.179 \pm 0.01 | 0.130 \pm 0.32 | -9.54 \pm 1.15 | -12.1 \pm 2.34 |
| F4P3 | 106.56 \pm 1.55 | 130.2 \pm 0.48 | 0.148 \pm 0.02 | 0.062 \pm 0.85 | -9.38 \pm 0.41 | -7.1 \pm 1.80 |
| F4P4 | 119.46 \pm 1.42 | 162.1 \pm 1.42 | 0.215 \pm 0.02 | 0.092 \pm 0.65 | -4.67 \pm 1.29 | -10.7 \pm 11.8 |

Table 3 Physicochemical stability results of the finalized CA-NE formulation (means \pm SD, n = 3).

| Formulation Code | Temp. | Time | Average Droplet Size (nm) | Polydispersity Index (PdI) | Zeta potential (mV) | pH | Conductivity (μ s/cm) | |
|------------------|-------|------|---------------------------|----------------------------|---------------------|-----------------|----------------------------|-----------------|
| F4P1 | 5 °C | T7 | 133.11 \pm 3.65 | 0.055 \pm 0.03 | -16.7 \pm 1.10 | 4.72 \pm 0.76 | 85.6 \pm 3.78 | |
| | | T30 | 131.45 \pm 1.00 | 0.050 \pm 0.01 | -13.6 \pm 0.87 | 4.70 \pm 2.50 | 84.0 \pm 3.43 | |
| | | T60 | 131.14 \pm 1.63 | 0.052 \pm 0.01 | -15.0 \pm 1.22 | 4.72 \pm 0.20 | 87.5 \pm 3.45 | |
| | 25 °C | T1 | 106.93 \pm 1.25 | 0.128 \pm 0.07 | -13.3 \pm 9.98 | 4.48 \pm 0.90 | 78.1 \pm 2.34 | |
| | | T7 | 121.00 \pm 0.30 | 0.132 \pm 0.30 | -9.1 \pm 1.17 | 4.56 \pm 0.54 | 96.1 \pm 1.24 | |
| | | T30 | 148.37 \pm 1.35 | 0.061 \pm 0.01 | -10.1 \pm 1.79 | 4.55 \pm 0.43 | 87.0 \pm 1.65 | |
| | 40 °C | T60 | 175.86 \pm 1.72 | 0.073 \pm 0.03 | -8.8 \pm 0.26 | 4.53 \pm 0.53 | 86.3 \pm 0.43 | |
| | | T7 | 161.08 \pm 2.13 | 0.071 \pm 0.01 | -8.9 \pm 2.00 | 4.79 \pm 0.45 | 90.1 \pm 7.74 | |
| | | T30 | 169.14 \pm 1.30 | 0.130 \pm 0.01 | -9.0 \pm 1.75 | 5.12 \pm 2.13 | 86.0 \pm 3.20 | |
| | | | T60 | 210.52 \pm 4.65 | 0.139 \pm 0.02 | -8.3 \pm 0.63 | 5.10 \pm 0.78 | 81.6 \pm 7.90 |

et al., 2021). In the present study, conductivity measurements were taken for a period of 60 days at predetermined time points for F4 series CA-NEs. The results displayed no substantial electrical conductivity changes in formulations at three different stability environments (Table 3).

Viscosity is an important parameter commonly used to evaluate the effect of stress conditions on emulsion stability. In addition, viscosity is related to the parameters that play a role in determining the quality of the formulation (Altuntaş and Yener, 2015). In this regard, viscosity measurements of F4 series NEs were monitored for 60 days. In this period, viscosity values of the four CA-NEs were found to be within appropriate limits, and no breakdown was monitored in consistency under overall stability conditions. Viscosity-based stability data of the finalized CA-NE formulation coded F4P1 were given in Fig. 2.

Active ingredient content analysis was a critical necessity for all kinds of dosage forms. The quantity of the active ingredient in the product should not deviate from the labeled quantity beyond certain specified limits within the formulation's shelf life (Altuntaş and Yener, 2017). In our study, CA content (%) was found to be $97.51 \pm 7.64\%$ on the day of production, and $93.39 \pm 8.35\%$, $94.76 \pm 5.49\%$ and $92.93 \pm 4.41\%$ after 60th day at three different stability environments, respectively (Table 4). The remaining CA (%) was found to be $> 90\%$ during the storage period at three different conditions. This result indicated that the finalized NE formulation could protect the loaded CA from the degradation.

Observation of the morphology of the finalized CA-NE formulation (F4P1) was performed by TEM. TEM confirmed the development of CA-NEs and validated the average droplet size achieved. TEM analysis also demonstrated that the droplets

were uniformly distributed and spherical, and no droplet agglomeration was monitored (Fig. 3).

3.5. Spectrophotometric analysis of CA

Analysis of CA was carried out by UV-vis Spectrometer (Shimadzu, Japan) at 324 nm detection wavelength according to the method described by Hosseini et al. (Hosseini et al., 2013). Ethanolic solutions of CA at increasing concentrations (0.20, 0.39, 0.78, 1.56, 3.125, 6.25, 12.50 μ g/mL) were prepared in triplicate and analyzed against the ethanol as a blank solution spectrophotometrically. Subsequently, the calibration curve was drawn using the obtained results, and the equation was determined (Fig. 1S).

3.6. In vitro release profile of CA-NEs

In vitro drug release study was exerted to evaluate the ability of finalized CA-NE formulation to control CA release once applied on the skin. The *in vitro* drug release profiles of the finalized CA-NE formulation was given in Fig. 4. According to results, after 24 h and 48 h, $88.90 \pm 5.73\%$ and $95.15 \pm 2.09\%$ of CA release obtained with the finalized NE formulation (F4P1), respectively. This result showed that the F4P1 releases CA in a controlled manner, and with a slow release rate over time.

3.7. AMES/Salmonella test

Although many genotoxicity tests are used to investigate the mutagenic activity of chemicals and drugs, the traditional

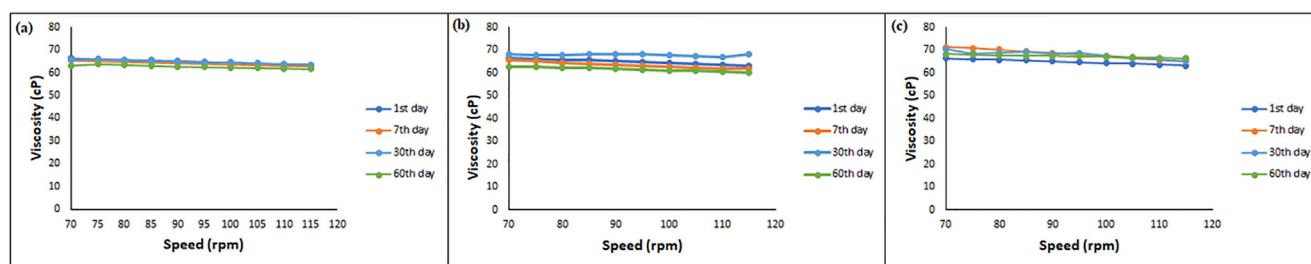


Fig. 2 Viscosity rheograms of the finalized CA-NE formulation during 60 days (a) 5 ± 3 °C; (b) 25 ± 2 °C and 60% RH; (c) 40 ± 2 °C and 75% RH.

Table 4 Drug remaining (%) of the finalized CA-NE formulation at varied storage conditions during physicochemical stability test period (means \pm SD, n = 3).

| Formulation Code | Storage Condition | Time | Remaining Drug Content (%) (n = 3) |
|------------------|-------------------------|------------------|------------------------------------|
| F4P1 | 5 \pm 3 °C | T30 | 92.47 \pm 6.91 |
| | | T60 | 93.39 \pm 8.35 |
| | 25 \pm 2 °C (% 65 RH) | T1 | 97.51 \pm 7.64 |
| | | T30 | 94.39 \pm 6.29 |
| | 40 \pm 2 °C (% 75 RH) | T60 | 94.76 \pm 5.49 |
| | | T30 | 91.10 \pm 3.17 |
| | T60 | 92.93 \pm 4.41 | |

Ames/Salmonella test is often preferred because it provides standard and reliable results (Maron and Ames, 1983, Wypij et al., 2020, Demir et al., 2020, Mortelmans and Zeiger, 2000, Guo et al., 2016, Du et al., 2019). Therefore, the genotoxicity of blank-NE, CA and the finalized CA-NE formulation was evaluated with the Ames/Salmonella test. The TA98 and TA100 mutant strains of *S. typhimurium* were used because they allow the identification of mutagens that cause a frameshift and base-pair substitution, respectively. The empty NE and CA-NE concentrations were used in this study as 0.25, 0.5 and 1 mg/plate. The concentration of CA was used as 0.004, 0.090 and 0.018 mg/plate according to the amount in 0.25, 0.5 and 1 mg/plate CA-NE. Results of the study were given in Table 5, Figs. S2 and S3. In conclusion, it was determined that the concentrations of blank NE and the finalized CA-NE formulation tested according to the method determined by Mortelmans and Zeiger, 2000 did not cause frameshift or base-pair substitution. Statistical analysis also confirmed that blank NE and the finalized CA-NE formulation were not mutagenic ($p > 0.05$).

There are many studies in which the Ames/Salmonella test is used for the genotoxic analysis of nanomaterials. Most of these studies reported that nanomaterials are not mutagenic (Egil et al., 2020, Warheit et al., 2007, Szendi and Varga, 2008, Balasubramanyam et al., 2010, Clift et al., 2013). As a result of our study, it was found that NEs were not mutagenic in the Ames/Salmonella test. There are studies in which nanomaterials cause weak mutagenic effects in the Ames/Salmonella test (Kumar et al., 2011, Maenosono et al., 2007). This situation may be due to the structure or concentration of the nanomaterials used.

3.8. *In vitro* cell viability, tyrosinase, and melanogenesis activity results

The cytotoxicity of finalized CA-NE formulation was evaluated by MTT assay on HaCaT cells to test its safety profile. Different concentrations of CA-NE tested did not have any cytotoxic effect on HaCaT cells compared to the control group ($p > 0.05$) and cell viability was over 90% (Fig. 5). Therefore, the same concentrations of finalized CA-NE formulation were used to evaluate the tyrosinase and melanogenesis activity.

Melanin is the substance that gives human skin color and is synthesized in melanosomes. (Beak et al., 2004, Park and Choi, 2017). Excess melanin causes skin disorders such as hyperpigmentation, melisma, and malignant melanoma (Panich et al., 2010, Heo et al., 2010). Tyrosinase is the key enzyme responsible for melanin synthesis. Therefore, tyrosinase activity has become the main target for the development of tyrosinase inhibitors in the cosmetic field (Cui et al., 2018, Roselan et al., 2020).

Recently, the natural compounds obtained from plants that have tyrosinase and melanogenesis activities have attracted the attention of researchers (Silva et al., 2022, Kim et al., 2022, Moon et al., 2022, Uto et al., 2022). However, the stability of the herbal ingredients and the efficacy of penetrating the skin should be improved. NEs offer unique properties to increase the stability of herbal ingredients and their penetration efficiency into the skin. In our study, the tyrosinase and melanogenesis activity of the finalized CA-NE formulation was evaluated by *in vitro* cell culture. B16 melanoma cells generated from C57BL/6J mice are a reliable cell model system for analyzing melanin synthesis. These cells are often used to evaluate skin-whitening drugs (Kim et al., 2022). Therefore, experiments were performed using the melanoma B16F0 cell line. The tyrosinase activities of the finalized CA-NE formulation at different concentrations are shown in Fig. 6 and the melanogenesis activities are shown in Fig. 7. According to results, it was found that the finalized CA-NE formulation caused a significant decrease in melanogenesis activity and tyrosinase activities compared to the control group ($p < 0.05$).

In a study examining the tyrosinase activity of quercetin-loaded olive oil nanoemulsion (QT-NE) to determine its potential to reduce skin hyperpigmentation, they reported that QT-NEs inhibited 56% of tyrosinase activity (Silva et al., 2022). It exhibited a higher anti-tyrosinase activity than our study (Table S1). Another study reported the tyrosinase activity and melanin production of adlay bran oil (ABO)-loaded NEs with a particle size of 150 nm for the anti-hyperpigmentation

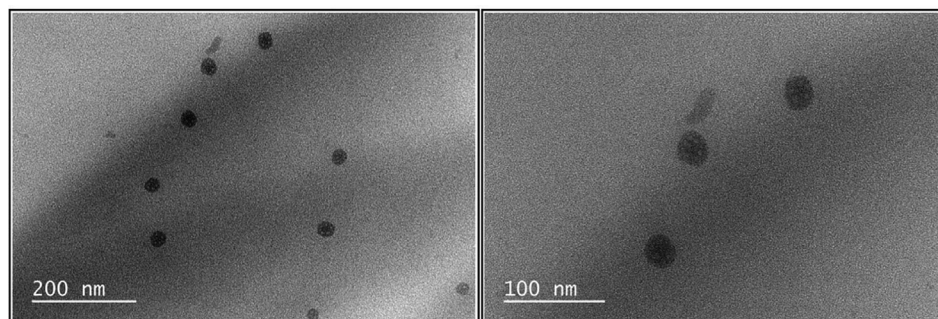


Fig. 3 TEM image of finalized CA-NE formulation.

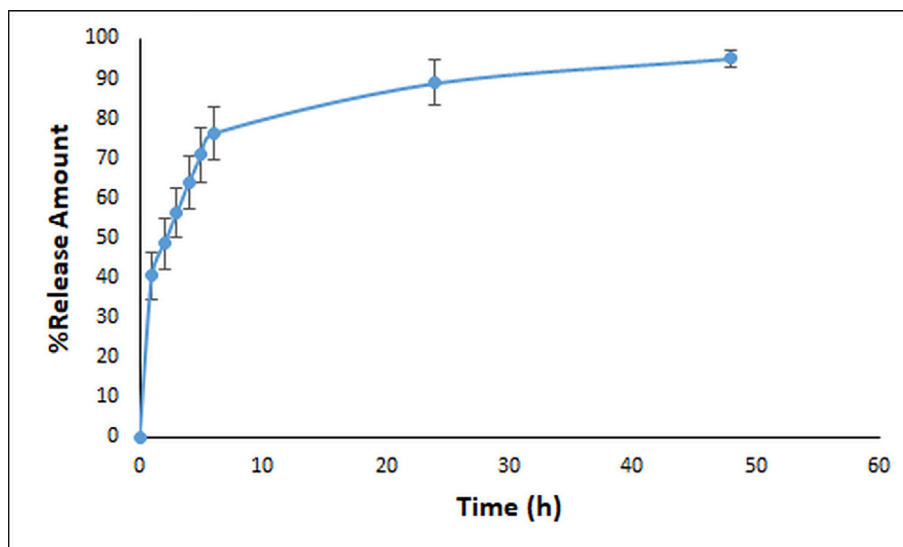


Fig. 4 *In vitro* release profile of the finalized CA-NE formulation (n = 3).

Table 5 Mutagenic effects of CA, blank-NE and the finalized CA-NE formulation on *S. typhimurium* TA98 and TA100 strains.

| Treatment | Concentration (mg/plate) | Number of revertant colony/Plate | |
|---------------------|--------------------------|----------------------------------|------------------------|
| | | TA98 Mean \pm SD | TA100 Mean \pm SD |
| Blank-NE | 0.25 | 28.66 \pm 6.50 | 75.66 \pm 6.02 |
| | 0.50 | 27.00 \pm 3.60 | 73.33 \pm 5.50 |
| | 1.00 | 26.00 \pm 4.58 | 77.00 \pm 5.56 |
| CA | 0.004 | 27.33 \pm 4.50 | 73.00 \pm 6.24 |
| | 0.009 | 26.33 \pm 6.11 | 72.00 \pm 2.00 |
| | 0.018 | 28.66 \pm 4.50 | 78.00 \pm 3.00 |
| | 0.25 | 27.00 \pm 2.64 | 73.00 \pm 2.00 |
| CA-NE | 0.50 | 29.00 \pm 3.60 | 76.33 \pm 5.03 |
| | 1.00 | 27.00 \pm 5.29 | 74.66 \pm 3.51 |
| | NPD | 10 ⁻² | 886.66 \pm 12.58* |
| Positive Control | SA | 10 ⁻³ | 993.66 \pm 13.65* |
| | Negative Control | | 29.00 \pm 7.93 |
| Spontaneous Control | | 27.00 \pm 7.54 | 72.66 \pm 2.08 |

NPD: 4-Nitro-o-phenylenediamine.

SA: Sodium azide.

* The mean revertant colony number difference between negative control and application groups is significant at the level of $p < 0.05$ (Tukey test).

activity of ABO-NEs were both dose-dependently decreased (Ting et al., 2019). In our study, a dose-related decrease was also observed. Asasutjarit et al., (2021) formulated andrographolide (AG) phytocomponent-loaded NE (AG-NE) isolated from *Andrographis paniculata* and evaluated its tyrosinase and melanogenesis activity. The results showed that it inhibited tyrosinase and melanogenesis activities (Asasutjarit et al., 2021).

3.9. Molecular docking and ADME results

Tyrosinase, a key enzyme in the melanogenesis pathway, is a copper-containing enzyme, responsible for developing melanin pigment. Tyrosinase inhibitors are the most common target for inhibiting this pathway (Adak, 2019, Chang, 2012). To determine the activity of tyrosinase inhibitors, kojic acid, hydroquinone or arbutin are generally used as references.

Therefore, the effectiveness of CA will be evaluated by comparing with the effectiveness of kojic acid. Fungal tyrosinase from *Agaricus bisporus* is used in tyrosinase inhibitor studies because it is very similar to mammalian tyrosinase and is usually available commercially in a pure form. Also, the effectiveness of CA on the human tyrosinase-related protein was investigated using tyrosinase-related protein 1 (TYRP1).

Firstly, to assess tyrosinase inhibitory activity mechanism of the investigated CA and kojic acid, the mushroom tyrosinase with 2.78 Å resolution of tetramer structure (PDB:2Y9X), which complexed with two H subunits which contains a binuclear copper coordinated with three histidine residues, ~392 residues, and two L subunits of ~150 residues was chosen as a receptor for docking analysis. The dimeric form having A and B chains crystal data of polyphenol oxidase with tetramer form belonging to *Agaricus bisporus* was preferred for more efficient docking calculations using the Swiss Model server.

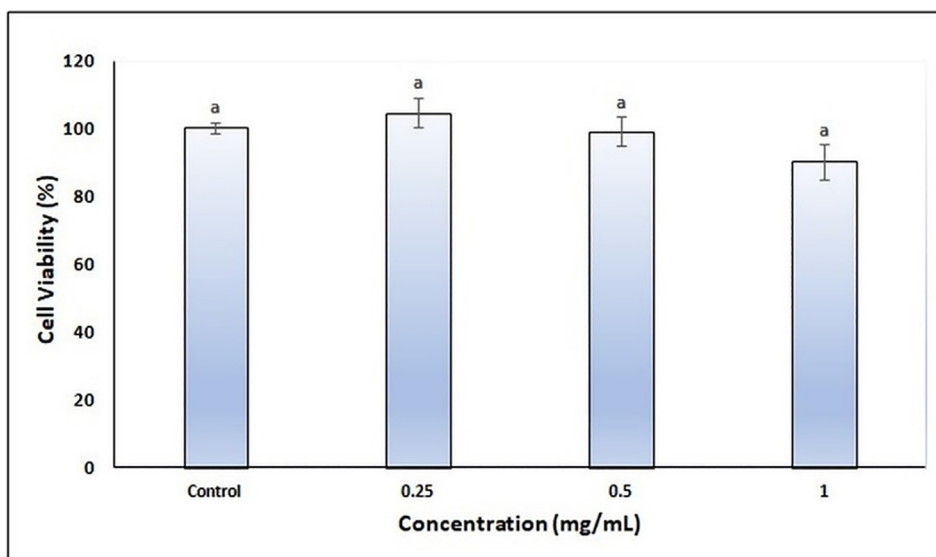


Fig. 5 Cell viability analysis of the finalized CA-NE formulation. (Different letters mean the significant difference between the control and treatment groups.).

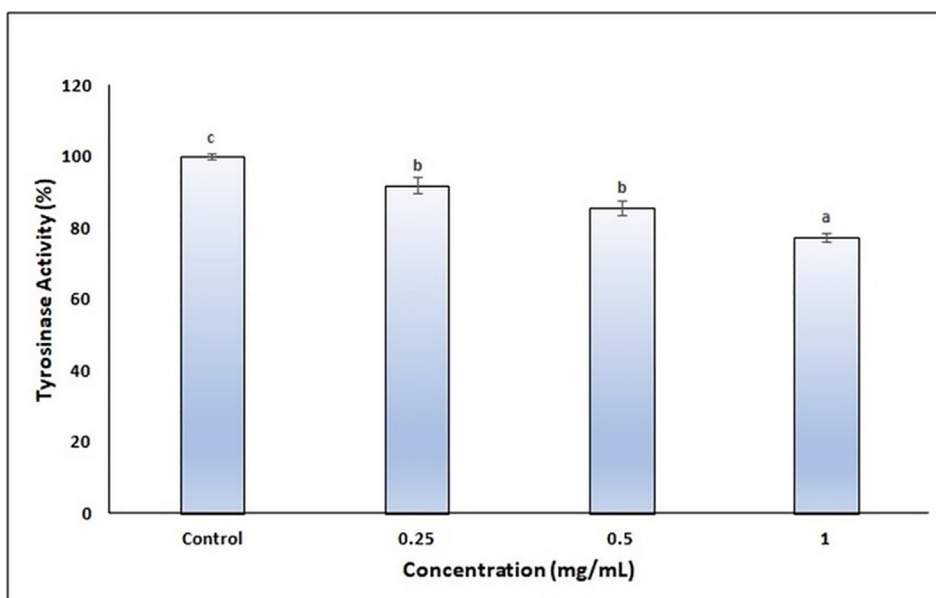


Fig. 6 Tyrosinase activity of the finalized CA-NE formulation.

Then, tyrosinase-associated protein 1 (TYRP1), one of three tyrosinase-like glycoenzymes that is key to the production of melanin, was chosen as another receptor to elicit CA activity. The crystal structure of human tyrosinase-related protein 1 (PDB:5M8L) has two zinc ions in the active site instead of the copper ions found in tyrosinases, which was also used as another receptor (Lai et al., 2017, Taslimi, 2020).

Since binding (chelation) with copper atoms is predicted to be important for antityrosinase activity, the fungal tyrosinase from *Agaricus bisporus* enzyme was prepared both with and without copper in order to show the effect of copper atoms,

and the binding mechanism with chlorogenic acid was investigated in both complex. In addition, the binding mechanism with kojic acid as a reference, which has the capacity to chelate with copper atoms, was also compared in this study.

The interaction, and binding energies of CA with the binding site of both copper and non-copper tyrosinase receptors were compared to determine the effect of copper atoms in the binding site of tyrosinase. The analyses revealed that CA directly interacts with the active site of both copper and non-copper tyrosinase enzymes and settled in its binding site. However, docking score energy of CA and tyrosinase with copper

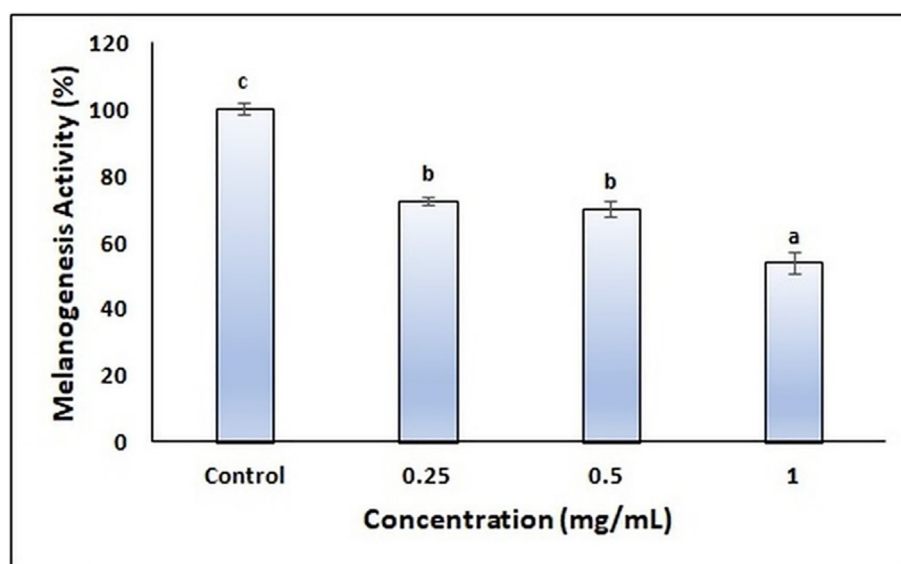


Fig. 7 Melanogenesis activity of the finalized CA-NE formulation.

ions was calculated as -7.80 kcal/mol, while with copper-free tyrosinase, a docking score of -6.72 kcal/mol was found. Copper ions located in the binding site of the tyrosinase enabled CA to bind more strongly and steadily to the receptor's binding side, like kojic acid.

The docking score energies of CA with both copper and non-copper tyrosinase receptors and kojic acid were given in Table 6 and seen in Fig. 8(a–c). The 2D docked pose of CA and binding pocketed interactions were depicted for both copper (a), non-copper tyrosinase receptor (b), kojic acid (c), and CA with human tyrosinase (d) were seen respectively in Fig. 8. The hydrophobic, polar, and positively charged residues in the binding region of the receptor were also given in Table 6 and Fig. 8.

As a result of the binding to the copper tyrosinase, the trihydroxycyclohexanecarboxylic acid group was directed toward the binding pocket. The interactions that support this orientation with the 2.06 Å hydrogen bonding between the polar ASN 259 residue and OH group, and at the same time, the 2.17 Å salt bridge between the Cu and the O⁻ atom provides stable bonding. In addition, the 1.76 Å hydrogen bond formed between the negatively charged GLU 321 residue and the OH group also supports this stable binding. The salt bridge interactions (2.17 Å and 3.60 Å) between Cu and O atoms give rise to the most stable binding at the lowest docking energy with -7.80 kcal/mol.

According to the docking analysis results of CA with the copper-free tyrosinase receptor, the hydrogen bonds with polar ASN 259 and positive charged ARG 267 residues with 2.78 Å, and 1.88 Å, respectively and a salt bridge with ARG267 residue with 1.54 Å bond lengths, and the distant interactions with HIS 60 and THR 260 at 4 Å and 4.26 Å, respectively, have been observed to contribute this binding. The hydroxy group displayed a vital role in anchoring with the enzyme.

This hydrogen bonding and salt bridge interactions between CA in the active site of the mushroom tyrosinase enzyme for both copper (a) and non-copper tyrosinase receptor (b) and kojic acid (c) and CA with human tyrosinase (d) were also seen in Fig. 9.

In the literature, tyrosinase inhibitory activity of some synthesized compounds or natural essential oils or extract were also evaluated using molecular docking analysis method. In one study, according to the results of computational docking studies of the compound with the most optimal binding mode with 2Y9X in the binding pocket of fungal tyrosinase, the docking score was calculated as -5.934 kcal/mol. Consistent interactions were shown between the hydroxyl and Cu ions in the active site for the most active compound. This compound was performed hydrogen bond interaction with ARG268 (Nazir et al., 2020). Wang et al. suggested that the melanin-reducing effects of Linderanolide B and subamolide A on human epidermal melanocytes might be due to their binding with copper ions in the tyrosinase active site, as indicated in the modeling program (Wang et al., 2011). In another study, it was reported that tyrosinase inhibitory activity of *Lippia origanoides* essential oils were also investigated. The results showed that all docked ligands were found to interact between an oxygen atom of the ligands and Cu or histidine residue (da Silva et al., 2017). Chen et al. reported that molecular docking analysis results of natural compounds T1 and T2 extracted from *Gastrodia elata* reveal that the sulfur atom of T1 interacting with copper ions in the active site of tyrosinase is crucial for its ability to inhibit fungal tyrosinase and disrupt human melanin synthesis (Chen et al., 2015). When the results of the molecular docking analysis for CA are evaluated, it can be said that CA has strong tyrosinase inhibitory activity due to the hydroxyl groups of CA, the hydrogen bond interactions with the binding site residues, and the electrostatic interactions between Cu ions.

Kojic acid has also been shown to interact with copper atoms in the active site of tyrosinase with salt bridge interactions and pi-pi stacking interactions with Histidine residues in Fig. 8(c). Compared to the effects of CA and kojic acid on the mushroom tyrosinase enzyme, considering the binding energies, CA was docked with a more stable binding energy (-7.80 kcal/mol) than kojic acid (-5.60 kcal/mol), which was formed by hydrogen bonds with OH groups and salt bridge interactions with Cu atoms. Based on the docking

Table 6 The docking score energies and probable interactions of CA with tyrosinase enzyme for both copper, and non-copper mushroom tyrosinase receptor with kojic acid and human tyrosinase receptor.

| Receptor | Mushroom tyrosinase Receptor (PdbID: 2Y9X) | | Human tyrosinase Receptor (PdbID: 5M8L) | |
|-----------------------------|--|--|--|--|
| | Chlorogenic Acid | | Kojic Acid | Chlorogenic Acid |
| Docking Score (Kcal/mol) | -7.80 | -6.72 | -5.60 | -4.53 |
| H.Bond (Angstrom) | ASN259(2.06)GLU321 (1.76) | ASN259(2.78)ARG267 (1.88) | - | ARG13(1.63)ARG13 (2.24)ARG13 (2.38)LEU68 (1.86)ASN72 (2.59) |
| Salt Bridge | Cu (2.17) | ARG267(1.54) | Cu (2.43)Cu (2.40) | ARG13(3.60) |
| Metal | Cu | - | Cu | |
| Pi-Pi Stacking | - | - | HIS84(4.61) HIS262 (4.13)HIS258 (5.06) | |
| Hydrophobic Residues | VAL247, ALA245, PHE263, MET279, VAL282, ALA285, PHE89, PHE291 | VAL247, MET256, PHE89, PHE263, ALA285, PHE291, VAL282, MET279, LEU274 | VAL247, PHE263, MET279, MET256, VAL282, PRO283, ALA285, ALA286, VAL298, CYS82, PHE89, TRP92, TYR96, PHE291 | PHE71, PHE79, LEU68, PRO67, TRP66, VAL65, ALA7, VAL9, ALA11, LEU12, MET16, ALA46, VAL44, ALA43, TRP420, PHE2, ILE145, LEU146, PHE155 |
| Polar Residues | HIS84, HIS295, HIS294, HIS60, HIS258, ASN259, HIS262, SER281, HIE243 | HIS84, HIE295, HIE243, HIS258, ASN259, THR260, HIS262, HIS60, SER281, HIE278 | HIS84, HIE295, HIE294, HIS284, ASN259, THR260, HIS258, HIS262, THR260, HIS60, SER281, HIE243 | THR74, ASN72, SER142, ASN151, THR8, SER14 |
| Charged (negative) Residues | GLU321 | GLU255 | GLU255 | GLU42, GLU64, ASP62, ASP61, GLU143, GLU10 |
| Charged (positive) Residues | - | ARG267 | ARG267 | ARG13, ARG73, ARG69, ARG141 |
| Glycine | GLY244, GLY280, GLY85 | GLY248, GLY280 | GLY85, GLY266, LY280 | GLY15, GLY150 |

results, it was observed that CA interacts directly with the mushroom tyrosinase enzyme, not only by hydrogen bonds, but also bonding with the copper ion in the active site of the enzyme, just like kojic acid. It is expected that CA is promising to anti-tyrosinase activity, which has a better binding energy than kojic acid which efficacy has been proven in clinical studies but has been limited in cosmetics due to its side effects (Desmedt et al., 2016).

For human tyrosinase enzyme, CA was also evaluated and compared with literature (Taslimi, 2020). In the study, in which the inhibition effects of six natural phenolic compounds against tyrosinase were summarized, the docking calculations of the molecules were used and the docking energies were found in the range of -6.37 kcal/mol at the lowest and -3.14 kcal/mol at the highest. It was concluded that CA formed a complex with the binding energy of -4.53 kcal/mol

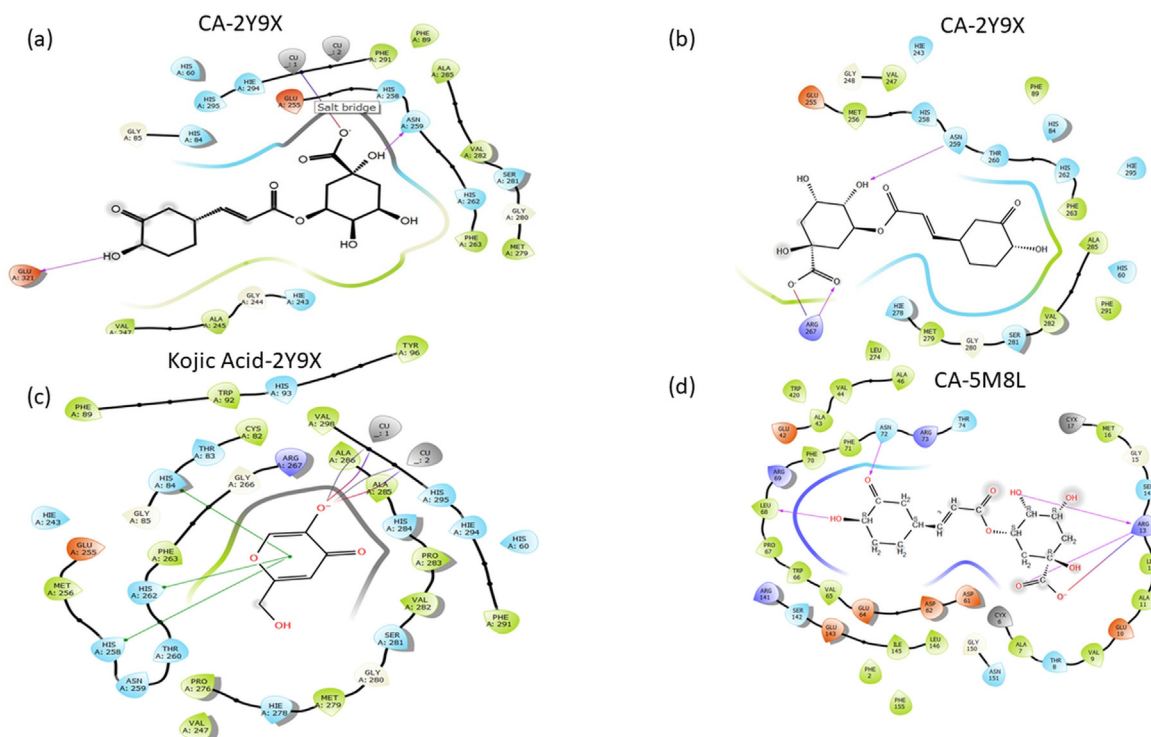


Fig. 8 The 2D docked pose of CA and binding pocket interactions were depicted for both copper (a), and non-copper tyrosinase receptor (b), kojic acid (c), and CA with human tyrosinase (d).

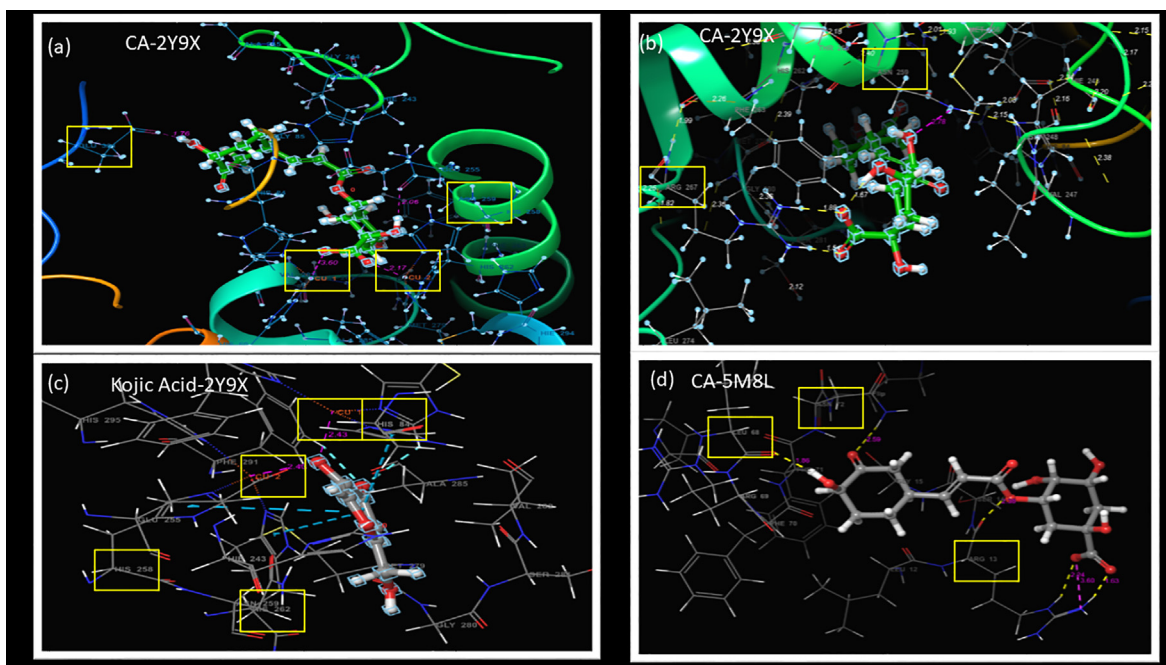


Fig. 9 The hydrogen bonding and salt bridge interactions between CA in the active site of the tyrosinase enzyme for both copper (a) and non-copper tyrosinase receptor (b) and kojic acid (c) and CA with human tyrosinase (d).

to the binding site of the human tyrosinase enzyme, and this complex was obtained by strong hydrogen binding to ARG13, ASN72 and LEU68 residues as seen in Figs. 8(d) and 9(d).

A comparison of the calculated pharmacokinetic properties of CA docked with both copper and non-copper tyrosinase receptor and kojic acid was also given in Table 7. The calculated the total solvent accessible surface area (Solute total

Table 7 The docking score energies and ADME properties of CA with tyrosinase enzyme for both copper, and non-copper tyrosinase receptor.

| Mushroom Tyrosinase Receptor Pdb ID: 2Y9X | | | | |
|---|------------------|--------------|------------|----------------------------------|
| | Chlorogenic Acid | | Kojic Acid | (Range 95% of Drugs) |
| <i>Docking Score(Kcal/mol)</i> | -7.80 | -6.72 | -5.60 | |
| Principal Descriptors | | | | |
| Solute Molecular Weight | 358.344 | 358.344 | 142.111 | (130.0 /725.0) |
| Solute Total SASA | 618.246 | 609.799 | 313.286 | (300.0 /1000.0) |
| Solute Hydrophobic SASA | 273.077 | 275.196 | 59.826 | (0.0 /750.0) |
| Solute Hydrophilic SASA | 334.985 | 322.633 | 160.698 | (7.0 /330.0) |
| Solute Carbon Pi SASA | 10.184 | 11.970 | 92.761 | (0.0/450.0) |
| Solute Weakly Polar SASA | 0.000 | 0.000 | 0.000 | (0.0 /175.0) |
| Solute Molecular Volume (A ³) | 1091.415 | 1075.223 | 472.797 | (500.0 /2000.0) |
| Solute vdW Polar SA (PSA) | 192.425 | 187.593 | 80.587 | (7.0 /200.0) |
| Solute No. of Rotatable Bonds | 8.000 | 8.000 | 3.000 | (0.0 /15.0) |
| Solute as Donor - Hydrogen Bonds | 5.000 | 5.000 | 2.000 | (0.0 /6.0) |
| Solute as Acceptor - Hydrogen Bonds | 11.850 | 11.850 | 4.950 | (2.0 /20.0) |
| Solute Globularity (Sphere = 1) | 0.829 | 0.832 | 0.937 | (0.75 /0.95) |
| Predictions for Properties: | | | | |
| QP Polarizability (Angstroms ³) | 32.485M | 31.854M | 11.727 | (13.0 /70.0) |
| QP log P for hexadecane/gas | 11.908M | 11.683M | 4.994 | (4.0/18.0) |
| QP log P for octanol/gas | 25.981M | 25.574M | 9.828 | (8.0 /35.0) |
| QP log P for water/gas | 20.785M | 20.693M | 9.340 | (4.0 /45.0) |
| QP log P for octanol/water | -0.745 | -0.736 | -0.592 | (-2.0/ 6.5) |
| QP log S for aqueous solubility | -2.702 | -2.601 | -0.372 | (-6.5/0.5) |
| P log S - conformation independent | -1.977 | -1.977 | -0.951 | (-6.5 /0.5) |
| QP log K hsa Serum Protein Binding | -0.949 | -0.970 | -0.861 | (-1.5/1.5) |
| QP log BB for brain/blood | -3.167 | -3.023 | -0.838 | (-3.0 /1.2) |
| No. of Primary Metabolites | 6 | 6 | 2 | (1.0 /8.0) |
| Predicted CNS Activity (- - to + +) | - | - | - | |
| HERG K+ Channel Blockage: log IC50 | -2.537 | -2.494 | -2.996M | (concern below -5) |
| Apparent Caco-2 Permeability (nm/sec) | 1 | 2 | 296 | (< 25 poor, > 500 great) |
| Apparent MDCK Permeability (nm/sec) | 0 | 0 | 132 | (< 25 poor, > 500 great) |
| QP log Kp for skin permeability | -6.889 | -6.655 | -3.866 | (Kp in cm/hr) |
| Jm, max transdermal transport rate | 0.000 | 0.000 | 6.055 | (micrograms/cm ² -hr) |
| Lipinski Rule of 5 Violations | 0 | 0 | 0 | (maximum is 4) |
| Jorgensen Rule of 3 Violations | 1 | 1 | 0 | (maximum is 3) |
| % Human Oral Absorption in GI (+ -20%) | 27 | 29 | 68 | (< 25% is poor) |
| Qual, Model for Human Oral Absorption | low | low | Medium | (> 80% is high) |

SASA), the total solvent accessible surface area on N, O, and H on heteroatoms (Hydrophilic SASA), total solvent-accessible volume (Molecular Volume), and Van der Waals surface area of polar nitrogen and oxygen atoms (PSA) values for CA docked with copper tyrosinase receptor were obtained at higher values than non-copper tyrosinase receptor. Also, predicted polarizability value, hexadecane/gas, octanol/gas, and water/gas values were calculated at higher for tyrosinase receptor with copper ions. Kojic acid with molecular formula C₆H₆O₄ has a molecular weight of 142.11 g/mol and has a 68% Human Oral Absorption value. However chlorogenic acid is not suitable for oral use, and its skin permeability value is suitable for only topical use. Considering the detailed results provided by molecular docking analysis and ADME calculations for CA with polyphenol ester groups similar to hydroxycinnamic acid structure provides the opportunity to be designed and used as a tyrosinase inhibitor for topical applications.

4. Conclusion

Although pigment disorders are seen as widespread dermatological problems, many issues, such as local or systemic side effects, toxicity, low stability, poor skin penetration and/or low efficacy, are encountered with agents used in treatment today. Therefore, these issues can be avoided by developing an appropriate dosage form containing natural actives, which have proven effective, have no harmful effects, and have low-cost production. In our study, stable CA-NEs with a desired physicochemical properties were obtained by ultrasonic homogenization for dermal usage in hyperpigmentation treatment for the first time. When F4 series formulations are evaluated during the 60-day stability test period, there is no significant difference concerning to particle size, PdI and zeta potential. Thus the F4P1 coded CA-NE formulation prepared with 15 min ultrasonication process without pre-emulsification step was selected due to the advantages such as energy saving and production efficiency. Also, its slow and controlled release are another advantage of the finalized CA-NE formulation. It was determined that the formulation was safe for transdermal application according to the *in vitro* cell viability results, the

Ames test results also supported these findings, and the formulation was not mutagenic. In efficacy experiments on Melanoma B16 cells, it was determined that the finalized CA-NE formulation reduced tyrosinase activity and melanogenesis activity.

The hydroxy group of CA displayed an essential role in anchoring with the enzyme. The hydrogen bond interactions of the hydroxyl groups with the residues in the active site and the interaction between Cu ions supported stable bonding. In addition, the oxygen atom forms salt bridges to aid in contact with copper ions, consistent with fundamental binding interactions between CA and tyrosinase enzyme. As a result, the antityrosinase activity of CA, a derivative of cinnamic acid, was evaluated by clarifying the mechanism of action on both mushroom tyrosinase and human tyrosinase enzymes comparing it kojic acid as a reference molecule. The molecular docking study and pharmacokinetic analyzes also showed that CA-NEs could serve as a potential drug to effectively for treatment of hyperpigmentation.

According to our *in vitro* and *in silico* findings, because of anti-tyrosinase and anti-melanogenesis efficacy, and safety profile with the non-mutagenic/non-toxic properties, chlorogenic acid nanoemulsion might be suggested as an innovative skin lightening formulation for cosmetic application.

Ethical approval

This article does not contain any studies with human participants or animals performed by any of the authors.

Acknowledgments

This study was supported by TUBITAK with the project numbered 117S097 and titled “Development of herbal nanoemulsions for the elimination of the hair graying problem, evaluation of the *in vivo* efficacy and safety”. The authors would thank TUBITAK for their support.

Conflicts of Interest

The authors declare no conflict of interest.

Appendix A. Supplementary material

Supplementary material to this article can be found online at <https://doi.org/10.1016/j.arabjc.2022.104362>.

References

- 10993-5, 2009. Biological evaluation of medical devices—Part 5: Tests for *in vitro* cytotoxicity. IOS, Switzerland.
- Abbas, S., Hayat, K., Karangwa, E., Bashari, M., Zhang, X., 2013. An overview of ultrasound-assisted food-grade nanoemulsions. *Food Eng. Rev.* 5, 139–157.
- Adak, T., 2019. Kojik asit türevi bileşiklerin tasarımı, sentezi ve melanoma hücrelerine karşı sitotoksiteleri ile tirozinaz inhibisyonu etkilerinin değerlendirilmesi.
- Adjonu, R., Doran, G., Torley, P., Agboola, S., 2014. Formation of whey protein isolate hydrolysate stabilised nanoemulsion. *Food Hydrocolloids* 41, 169–177.
- Agbai, O.N., Taylor, S.C., 2015. Melasma and depigmentation agents. *Cosmeceut. Active Cosmet.* 343.
- Ali, S.M., Yosipovitch, G., 2013. Skin pH: from basic science to basic skin care. *Acta Dermato-Venereologica* 93, 261–269.
- Altuntaş, E., Yener, G., 2015. Anti-aging potential of a cream containing herbal oils and honey: Formulation and *in vivo* evaluation of effectiveness using non-invasive biophysical techniques. *IOSR J. Pharm. Biol. Sci.* 10, 51–60.
- Altuntaş, E., Yener, G., 2017. Formulation and evaluation of thermoreversible *in situ* nasal gels containing mometasone furoate for allergic rhinitis. *AAPS PharmSciTech* 18, 2673–2682.
- Altuntaş, E., Yener, G., Özkan, B., 2019. Nanocarriers Systems and Their Application for the Delivery of Different Phytoconstituents. *Novel Drug Delivery Syst. Phytoconstituents* 9.
- Arbain, N., Basri, M., Salim, N., Wui, W., Rahman, M.A., 2018. Development and characterization of aerosol nanoemulsion system encapsulating low water soluble quercetin for lung cancer treatment. *Mater. Today: Proc.* 5, S137–S142.
- Asasutjarit, R., Sooksai, N., Fristiohady, A., Lairrungruang, K., Ng, S.-F., Fuongfuchat, A., 2021. Optimization of production parameters for andrographolide-loaded nanoemulsion preparation by microfluidization and evaluations of its bioactivities in skin cancer cells and uvb radiation-exposed skin. *Pharmaceutics* 13, 1290.
- Azarmi, S., Roa, W., Löbenberg, R., 2007. Current perspectives in dissolution testing of conventional and novel dosage forms. *Int. J. Pharm.* 328, 12–21.
- Balasubramanyam, A., Sailaja, N., Mahboob, M., Rahman, M., Hussain, S.M., Grover, P., 2010. *In vitro* mutagenicity assessment of aluminium oxide nanomaterials using the Salmonella/microsome assay. *Toxicol. In Vitro* 24, 1871–1876.
- Bassoli, B.K., Cassolla, P., Borba-Murad, G.R., Constantin, J., Salgueiro-Pagadigorria, C.L., Bazotte, R.B., da Silva, R.S.D.S.F., De Souza, H.M., 2008. Chlorogenic acid reduces the plasma glucose peak in the oral glucose tolerance test: effects on hepatic glucose release and glycaemia. *Cell Biochem. Funct.: Cell. Biochem. Modulat. Active Agents Dis.* 26, 320–328.
- Baumann, L.S., Baumann, L., 2009. *Cosmetic dermatology*. McGraw-Hill Professional Publishing.
- Beak, S.M., Lee, Y.S., Kim, J.-A., 2004. NADPH oxidase and cyclooxygenase mediate the ultraviolet B-induced generation of reactive oxygen species and activation of nuclear factor- κ B in HaCaT human keratinocytes. *Biochimie* 86, 425–429.
- Bernardi, D.S., Pereira, T.A., Maciel, N.R., Bortoloto, J., Viera, G. S., Oliveira, G.C., Rocha-Filho, P.A., 2011. Formation and stability of oil-in-water nanoemulsions containing rice bran oil: *in vitro* and *in vivo* assessments. *J. Nanobiotechnol.* 9, 1–9.
- Bienert, S., Waterhouse, A., de Beer, T.A., Tauriello, G., Studer, G., Bordoli, L., Schwede, T., 2017. The SWISS-MODEL Repository—new features and functionality. *Nucleic Acids Res.* 45, D313–D319.
- Bonita, J.S., Mandarano, M., Shuta, D., Vinson, J., 2007. Coffee and cardiovascular disease: *in vitro*, cellular, animal, and human studies. *Pharmacol. Res.* 55, 187–198.
- Budama-Kilinc, Y., Kecel-Gunduz, S., Ozdemir, B., Bicak, B., Akman, G., Arvas, B., Aydogan, F., Yolacan, C., 2020. New nanodrug design for cancer therapy: Its synthesis, formulation, *in vitro* and *in silico* evaluations. *Arch. Pharm.* 353, 2000137.
- Bugaj, A.M., 2015. Intradermal delivery of active cosmeceutical ingredients. *Novel Delivery Syst. Transdermal Intradermal Drug Delivery I*.
- Caddeo, C., Teskač, K., Sinico, C., Kristl, J., 2008. Effect of resveratrol incorporated in liposomes on proliferation and UV-B protection of cells. *Int. J. Pharm.* 363, 183–191.
- Chaiyana, W., Anuchapreeda, S., Somwongin, S., Marsup, P., Lee, K.-H., Lin, W.-C., Lue, S.-C., 2020. Dermal delivery enhancement of natural anti-ageing compounds from *Ocimum sanctum* Linn. extract by nanostructured lipid carriers. *Pharmaceutics* 12, 309.
- Chanchal, D., Swarnlata, S., 2008. Novel approaches in herbal cosmetics. *J. Cosmetic Dermatol.* 7, 89–95.
- Chang, T.-S., 2012. Natural melanogenesis inhibitors acting through the down-regulation of tyrosinase activity. *Materials* 5, 1661–1685.
- Chen, W.-C., Tseng, T.-S., Hsiao, N.-W., Lin, Y.-L., Wen, Z.-H., Tsai, C.-C., Lee, Y.-C., Lin, H.-H., Tsai, K.-C., 2015. Discovery of highly potent tyrosinase inhibitor, T1, with significant anti-

- melanogenesis ability by zebrafish in vivo assay and computational molecular modeling. *Sci. Rep.* 5, 1–8.
- Chinnici, F., Bendini, A., Gaiani, A., Riponi, C., 2004. Radical scavenging activities of peels and pulps from cv. Golden Delicious apples as related to their phenolic composition. *J. Agric. Food. Chem.* 52, 4684–4689.
- Clift, M.J., Raemy, D.O., Endes, C., Ali, Z., Lehmann, A.D., Brandenberger, C., Petri-Fink, A., Wick, P., Parak, W.J., Gehr, P., 2013. Can the Ames test provide an insight into nano-object mutagenicity? Investigating the interaction between nano-objects and bacteria. *Nanotoxicology* 7, 1373–1385.
- CSID:3708, 2022. Search ChemSpider [Online]. Available: <http://www.chemspider.com/Chemical-Structure.3708.html> [Accessed].
- Cui, H.-X., Duan, F.-F., Jia, S.-S., Cheng, F.-R., Yuan, K., 2018. Antioxidant and Tyrosinase Inhibitory Activities of Seed Oils from *Torreya grandis* Fort. ex Lindl. *BioMed Res. Int.* 2018.
- Curto, E.V., Kwong, C., Hermersdörfer, H., Glatt, H., Santis, C., Virador, V., Hearing Jr, V.J., Dooley, T.P., 1999. Inhibitors of mammalian melanocyte tyrosinase: in vitro comparisons of alkyl esters of gentisic acid with other putative inhibitors. *Biochem. Pharmacol.* 57, 663–672.
- da Silva, A.P., Silva, N.D.F., Andrade, E.H.A., Gratieri, T., Setzer, W.N., Maia, J.G.S., da Silva, J.K.R., 2017. Tyrosinase inhibitory activity, molecular docking studies and antioxidant potential of chemotypes of *Lippia origanoides* (Verbenaceae) essential oils. *PLoS ONE* 12, e0175598.
- de Freitas, M.M., Fontes, P.R., Souza, P.M., William Fagg, C., Neves Silva Guerra, E., de Medeiros Nóbrega, Y.K., Silveira, D., Fonseca-Bazzo, Y., Simeoni, L.A., Homem-de-Mello, M., 2016. Extracts of *Morus nigra* L. leaves standardized in chlorogenic acid, rutin and isoquercitrin: tyrosinase inhibition and cytotoxicity. *PLoS ONE* 11, e0163130.
- Demir, E., Qin, T., Li, Y., Zhang, Y., Guo, X., Ingle, T., Yan, J., Orza, A.I., Biris, A.S., Ghorai, S., 2020. Cytotoxicity and genotoxicity of cadmium oxide nanoparticles evaluated using in vitro assays. *Mutation Res./Genet. Toxicol. Environ. Mutagenesis* 850, 503149.
- Desmedt, B., Courselle, P., de Beer, J., Rogiers, V., Grosber, M., Deconinck, E., de Paepe, K., 2016. Overview of skin whitening agents with an insight into the illegal cosmetic market in Europe. *J. Eur. Acad. Dermatol. Venereol.* 30, 943–950.
- di Petrillo, A., González-Paramás, A.M., Era, B., Medda, R., Pintus, F., Santos-Buelga, C., Fais, A., 2016. Tyrosinase inhibition and antioxidant properties of *Asphodelus microcarpus* extracts. *BMC Complement. Alternat. Med.* 16, 1–9.
- Diane, J.M.M., Burgess, J., 2014. Vitamin E nanoemulsions characterization and analysis. *Int. J. Pharm.* 465, 455–463.
- Dickinson, E., Golding, M., 1997. Rheology of sodium caseinate stabilized oil-in-water emulsions. *J. Colloid Interface Sci.* 191, 166–176.
- Du, X., Gao, S., Hong, L., Zheng, X., Zhou, Q., Wu, J., 2019. Genotoxicity evaluation of titanium dioxide nanoparticles using the mouse lymphoma assay and the Ames test. *Mutation Res./Genet. Toxicol. Environ. Mutagenesis* 838, 22–27.
- Egil, A.C., Ozdemir, B., Gok, B., Kecel-Gunduz, S., Budama-Kilinc, Y., 2020. Synthesis, characterization, biological activities and molecular docking of *Epilobium parviflorum* aqueous extract loaded chitosan nanoparticles. *Int. J. Biol. Macromol.* 161, 947–957.
- Friesner, R.A., Banks, J.L., Murphy, R.B., Halgren, T.A., Klicic, J. J., Mainz, D.T., Repasky, M.P., Knoll, E.H., Shelley, M., Perry, J. K., 2004. Glide: a new approach for rapid, accurate docking and scoring. 1. Method and assessment of docking accuracy. *J. Med. Chem.* 47, 1739–1749.
- Frisch, M., Trucks, G., Schlegel, H., Scuseria, G., Robb, M., Cheeseman, J., Scalmani, G., Barone, V., Mennucci, B., Petersson, G., 2010. Gaussian 09 (revision C. 01) Inc. Wallingford CT.
- Gandhi, V., Verma, P., Naik, G., 2012. Exogenous ochronosis after prolonged use of topical hydroquinone (2%) in a 50-year-old Indian female. *Indian J. Dermatol.* 57, 394.
- García-Gavín, J., González-Vilas, D., Fernández-Redondo, V., Toribio, J., 2010. Pigmented contact dermatitis due to kojic acid. A paradoxical side effect of a skin lightener. *Contact Dermatitis* 62, 63–64.
- Ghazy, O., Fouad, M., Saleh, H., Kholif, A., Morsy, T., 2021. Ultrasound-assisted preparation of anise extract nanoemulsion and its bioactivity against different pathogenic bacteria. *Food Chem.* 341, 128259.
- Guo, X., Li, Y., Yan, J., Ingle, T., Jones, M.Y., Mei, N., Boudreau, M.D., Cunningham, C.K., Abbas, M., Paredes, A.M., 2016. Size- and coating-dependent cytotoxicity and genotoxicity of silver nanoparticles evaluated using in vitro standard assays. *Nanotoxicology* 10, 1373–1384.
- Guzelmeric, E., Ugurlu, P., Celik, C., Sen, N.B., Helvacioğlu, S., Charehsaz, M., Erdogan, M., Ockun, M.A., Kirmizibekmez, H., Aydin, A., 2022. *Myrtus communis* L. (Myrtle) plant parts: Comparative assessment of their chemical compositions, antioxidant, anticancer, and antimutagenic activities. *S. Afr. J. Bot.* 150, 711–720.
- Halgren, T.A., Murphy, R.B., Friesner, R.A., Beard, H.S., Frye, L. L., Pollard, W.T., Banks, J.L., 2004. Glide: a new approach for rapid, accurate docking and scoring. 2. Enrichment factors in database screening. *J. Med. Chem.* 47, 1750–1759.
- Harder, E., Damm, W., Maple, J., Wu, C., Reboul, M., Xiang, J.Y., Wang, L., Lupyan, D., Dahlgren, M.K., Knight, J.L., 2016. OPLS3: a force field providing broad coverage of drug-like small molecules and proteins. *J. Chem. Theory Comput.* 12, 281–296.
- Hastings, J., Owen, G., Dekker, A., Ennis, M., Kale, N., Muthukrishnan, V., Turner, S., Swainston, N., Mendes, P., Steinbeck, C., 2016. ChEBI in 2016: Improved services and an expanding collection of metabolites. *Nucleic Acids Res.* 44, D1214–D1219.
- Heo, S.-J., Ko, S.-C., Kang, S.-M., Cha, S.-H., Lee, S.-H., Kang, D.-H., Jung, W.-K., Affan, A., Oh, C., Jeon, Y.-J., 2010. Inhibitory effect of diphloretohydroxycarmalol on melanogenesis and its protective effect against UV-B radiation-induced cell damage. *Food Chem. Toxicol.* 48, 1355–1361.
- Hergueta-Castillo, M. E., López-Ruiz, R., Romero-González, R., Garrido Frenich, A., 2022. Non-Targeted Analysis of Co-Formulants in Antifungal Pesticide Formulations by Gas Chromatography-Tandem High Resolution Mass Spectrometry. Available at SSRN 4071340.
- Hosseini, S.F., Zandi, M., Rezaei, M., Farahmandghavi, F., 2013. Two-step method for encapsulation of oregano essential oil in chitosan nanoparticles: preparation, characterization and in vitro release study. *Carbohydr. Polym.* 95, 50–56.
- Ibarra-Berumen, J., Moreno-Eutimio, M.A., Rosales-Castro, M., Ordaz-Pichardo, C., 2022. Cytotoxic effect and induction of apoptosis in human cervical cancer cells by a wood extract from *Prosopis laevigata*. *Drug Chem. Toxicol.* 1–13.
- Ismaya, W.T., Rozeboom, H.J., Weijn, A., Mes, J.J., Fusetti, F., Wichers, H.J., Dijkstra, B.W., 2011. Crystal structure of *Agaricus bisporus* mushroom tyrosinase: identity of the tetramer subunits and interaction with tropolone. *Biochemistry* 50, 5477–5486.
- Jiang, J., Mei, Z., Xu, J., Sun, D., 2013. Effect of inorganic electrolytes on the formation and the stability of water-in-oil (W/O) emulsions. *Colloids Surf., A* 429, 82–90.
- Jin, U.-H., Lee, J.-Y., Kang, S.-K., Kim, J.-K., Park, W.-H., Kim, J.-G., Moon, S.-K., Kim, C.-H., 2005. A phenolic compound, 5-caffeoylquinic acid (chlorogenic acid), is a new type and strong matrix metalloproteinase-9 inhibitor: isolation and identification from methanol extract of *Euonymus alatus*. *Life Sci.* 77, 2760–2769.
- Karthik, P., Anandharamkrishnan, C., 2016. Fabrication of a nutrient delivery system of docosahexaenoic acid nanoemulsions via high energy techniques. *RSC Adv.* 6, 3501–3513.

- Kentish, S., Wooster, T., Ashokkumar, M., Balachandran, S., Mawson, R., Simons, L., 2008. The use of ultrasonics for nanoemulsion preparation. *Innovative Food Sci. Emerg. Technol.* 9, 170–175.
- Khalil, H., Alqahtani, N., Darrag, H., Ibrahim, H., Emeka, P., Badger-Emeka, L., Matsunami, K., Shehata, T., Elsewedy, H., 2021. Date palm extract (*Phoenix dactylifera*) PEGylated nanoemulsion: Development, optimization and cytotoxicity evaluation. *Plants* 10 (4).
- Kildaci, I., Budama-Kilinc, Y., Kecel-Gunduz, S., Altuntas, E., 2021. Linseed Oil Nanoemulsions for treatment of Atopic Dermatitis disease: Formulation, characterization, in vitro and in silico evaluations. *J. Drug Delivery Sci. Technol.* 64, 102652.
- Kim, J., Hwang, J.-S., Cho, Y.-K., Han, Y., Jeon, Y.-J., Yang, K.-H., 2001. Protective effects of (–)-epigallocatechin-3-gallate on UVA- and UVB-induced skin damage. *Skin Pharmacol. Physiol.* 14, 11–19.
- Kim, J.H., Kim, T.I., Ma, J.-Y., 2022. Synergistic effects of novel herbal decoctions from *Panax ginseng* and *Morus alba* on tyrosinase activity and melanogenesis in vitro. *Heliyon* 8, e08866.
- Kitagawa, S., Yoshii, K., Morita, S.-Y., Teraoka, R., 2011. Efficient topical delivery of chlorogenic acid by an oil-in-water microemulsion to protect skin against UV-induced damage. *Chem. Pharm. Bull.* 59, 793–796.
- Kumar, A., Pandey, A.K., Singh, S.S., Shanker, R., Dhawan, A., 2011. Cellular uptake and mutagenic potential of metal oxide nanoparticles in bacterial cells. *Chemosphere* 83, 1124–1132.
- Lai, X., Wichers, H.J., Soler-Lopez, M., Dijkstra, B.W., 2017. Structure of human tyrosinase related protein 1 reveals a binuclear zinc active site important for melanogenesis. *Angew. Chem. Int. Ed.* 56, 9812–9815.
- Li, H.-R., Habasi, M., Xie, L.-Z., Aisa, H.A., 2014. Effect of chlorogenic acid on melanogenesis of B16 melanoma cells. *Molecules* 19, 12940–12948.
- Liao, S., Yang, G., Wang, Z., Ou, Y., Huang, S., Li, B., Li, A., Kan, J., 2022. Ultrasonic preparation of Tween-essential oil (*Zanthoxylum schinifolium* Sieb. et Zucc) oil/water nanoemulsion: Improved stability and alleviation of *Staphylococcus epidermidis* biofilm. *Ind. Crops Prod.* 188, 115654.
- Maenosono, S., Suzuki, T., Saita, S., 2007. Mutagenicity of water-soluble FePt nanoparticles in Ames test. *J. Toxicol. Sci.* 32, 575–579.
- Mahdi Jafari, S., He, Y., Bhandari, B., 2006. Nano-emulsion production by sonication and microfluidization—a comparison. *Int. J. Food Prop.* 9, 475–485.
- Maron, D.M., Ames, B.N., 1983. Revised methods for the Salmonella mutagenicity test. *Mutation Res./Environ. Mutagenesis Related Subj.* 113, 173–215.
- Menezes, J.C., Kamat, S.P., Cavaleiro, J.A., Gaspar, A., Garrido, J., Borges, F., 2011. Synthesis and antioxidant activity of long chain alkyl hydroxycinnamates. *Eur. J. Med. Chem.* 46, 773–777.
- Miceli, N., Taviano, M., Giuffrida, D., Trovato, A., Tzakou, O., Galati, E., 2005. Anti-inflammatory activity of extract and fractions from *Nepeta sibthorpii* Benth. *J. Ethnopharmacol.* 97, 261–266.
- Miliovsky, M., Svinyarov, I., Mitrev, Y., Evstatieva, Y., Nikolova, D., Chochkova, M., Bogdanov, M.G., 2013. A novel one-pot synthesis and preliminary biological activity evaluation of cis-restricted polyhydroxy stilbenes incorporating protocatechuic acid and cinnamic acid fragments. *Eur. J. Med. Chem.* 66, 185–192.
- Moon, K.M., Yang, J.-H., Lee, M.-K., Kwon, E.-B., Baek, J., Hwang, T., Kim, J.-I., Lee, B., 2022. Maclurin Exhibits Antioxidant and Anti-Tyrosinase Activities, Suppressing Melanogenesis. *Antioxidants* 11, 1164.
- Mortelmans, K., Zeiger, E., 2001. The Ames Salmonella/microsome mutagenicity assay. *Mutation Res./Fundam. Mol. Mech. Mutagenesis* 455, 29–60.
- Muhammad, K.W., Akhtar, N., Haji, M., Mustafa, R., Murtaza, G., 2014. Stability study of a cosmetic emulsion loaded with *Tamarindus indica* seeds extract. *Lat. Am. J. Pharm.* 33, 731–738.
- Nazir, Y., Saeed, A., Rafiq, M., Afzal, S., Ali, A., Latif, M., Zuegg, J., Hussein, W.M., Fercher, C., Barnard, R.T., 2020. Hydroxyl substituted benzoic acid/cinnamic acid derivatives: Tyrosinase inhibitory kinetics, anti-melanogenic activity and molecular docking studies. *Bioorg. Med. Chem. Lett.* 30, 126722.
- Ngan, C.L., Basri, M., Lye, F.F., Masoumi, H.R.F., Tripathy, M., Karjiban, R.A., Abdul-Malek, E., 2014. Comparison of Box-Behnken and central composite designs in optimization of fullerene loaded palm-based nano-emulsions for cosmeceutical application. *Ind. Crops Prod.* 59, 309–317.
- Nikovska, K., 2012. Study of olive oil-in-water emulsions with protein emulsifiers. *Emirates J. Food Agric.*, 17–24.
- Ozkan, B., Altuntas, E., Cakir Koc, R., Budama-Kilinc, Y., 2022. Development of piperine nanoemulsions: an alternative topical application for hypopigmentation. *Drug Dev. Ind. Pharm.* 48, 117–127.
- Pacheco, M.T., Silva, A.C., Nascimento, T.L., Diniz, D.G., Valadares, M.C., Lima, E.M., 2019. Protective effect of cupira oil nanoemulsion against oxidative stress in UVA-irradiated HaCaT cells. *J. Pharm. Pharmacol.* 71, 1532–1543.
- Panich, U., Kongtaphan, K., Onkkoong, T., Jaemsak, K., Phadungrakwittaya, R., Thaworn, A., Akarasereenont, P., Wongkajornsilp, A., 2010. Modulation of antioxidant defense by *Alpinia galanga* and *Curcuma aromatica* extracts correlates with their inhibition of UVA-induced melanogenesis. *Cell Biol. Toxicol.* 26, 103–116.
- Panzella, L., Napolitano, A., 2019. Natural and bioinspired phenolic compounds as tyrosinase inhibitors for the treatment of skin hyperpigmentation: Recent advances. *Cosmetics* 6, 57.
- Park, E.-J., Choi, J.-I., 2017. Melanogenesis inhibitory effect of low molecular weight fucoidan from *Undaria pinnatifida*. *J. Appl. Phycol.* 29, 2213–2217.
- Pongsumpun, P., Iwamoto, S., Siripatrawan, U., 2020. Response surface methodology for optimization of cinnamon essential oil nanoemulsion with improved stability and antifungal activity. *Ultrason. Sonochem.* 60, 104604.
- Rajitha, P., Shammika, P., Aiswarya, S., Gopikrishnan, A., Jayakumar, R., Sabitha, M., 2019. Chaulmoogra oil based methotrexate loaded topical nanoemulsion for the treatment of psoriasis. *J. Drug Delivery Sci. Technol.* 49, 463–476.
- Romes, N.B., Abdul Wahab, R., Abdul Hamid, M., Oyewusi, H.A., Huda, N., Kobun, R., 2021. Thermodynamic stability, in-vitro permeability, and in-silico molecular modeling of the optimal *Elaeis guineensis* leaves extract water-in-oil nanoemulsion. *Sci. Rep.* 11, 1–19.
- Roselan, M.A., Ashari, S.E., Faujan, N.H., Mohd Faudzi, S.M., Mohamad, R., 2020. An improved nanoemulsion formulation containing Kojic Monooleate: Optimization, characterization and in vitro studies. *Molecules* 25, 2616.
- Sabouri, M., Samadi, A., Nasrollahi, S.A., Farboud, E.S., Mirrahimi, B., Hassanzadeh, H., Kashani, M.N., Dinarvand, R., Firooz, A., 2018. Tretinoin loaded nanoemulsion for acne vulgaris: Fabrication, physicochemical and clinical efficacy assessments. *Skin Pharmacol. Physiol.* 31, 316–323.
- Sarheed, O., Dibi, M., Ramesh, K.V., 2020. Studies on the Effect of Oil and Surfactant on the Formation of Alginate-Based O/W Lidocaine Nanocarriers Using Nanoemulsion Template. *Pharmaceutics* 12, 1223.
- Sastry, G.M., Adzhigirey, M., Day, T., Annabhimoju, R., Sherman, W., 2013. Protein and ligand preparation: parameters, protocols, and influence on virtual screening enrichments. *J. Comput. Aided Mol. Des.* 27, 221–234.
- Schrödinger 2020. Schrödinger Release 2020-1: QikProp. Schrödinger, LLC.

- Schrodinger, L., 2019. Small-Molecule Drug Discovery Suite 2019-3. 2017. Schrodinger LLC., New York, NY.
- Shakeel, F., Ramadan, W., Ahmed, M.A., 2009. Investigation of true nanoemulsions for transdermal potential of indomethacin: characterization, rheological characteristics, and ex vivo skin permeation studies. *J. Drug Target.* 17, 435–441.
- Shi, Y., Chen, Q.-X., Wang, Q., Song, K.-K., Qiu, L., 2005. Inhibitory effects of cinnamic acid and its derivatives on the diphenolase activity of mushroom (*Agaricus bisporus*) tyrosinase. *Food Chem.* 92, 707–712.
- Silva, C.C., Benati, R.B., Massaro, T.N., Pereira, K.C., Gaspar, L. R., Marcato, P.D., 2022. Antioxidant and anti-tyrosinase activities of quercetin-loaded olive oil nanoemulsion as potential formulation for skin hyperpigmentation. *J. Dispersion Sci. Technol.*, 1–11
- Silva, K.C.G., Sato, A.C.K., 2019. Sonication technique to produce emulsions: The impact of ultrasonic power and gelatin concentration. *Ultrason. Sonochem.* 52, 286–293.
- Søndergaard, C.R., Olsson, M.H., Rostkowski, M., Jensen, J.H., 2011. Improved treatment of ligands and coupling effects in empirical calculation and rationalization of pKa values. *J. Chem. Theory Comput.* 7, 2284–2295.
- Sonneville-Aubrun, O., Simonnet, J.-T., L'Alloret, F., 2004. Nanoemulsions: a new vehicle for skincare products. *Adv. Colloid Interface Sci.* 108, 145–149.
- Souza, P.M., Elias, S.T., Simeoni, L.A., de Paula, J.E., Gomes, S.M., Guerra, E.N.S., Fonseca, Y.M., Silva, E.C., Silveira, D.M., Magalhaes, P.O., 2012. Plants from Brazilian Cerrado with potent tyrosinase inhibitory activity. *PLoS ONE* 7, e48589.
- Szendi, K., Varga, C., 2008. Lack of genotoxicity of carbon nanotubes in a pilot study. *Anticancer Res.* 28, 349–352.
- Tadros, T., Izquierdo, P., Esquena, J., Solans, C., 2004. Formation and stability of nano-emulsions. *Adv. Colloid Interface Sci.* 108, 303–318.
- Takegami, S., Kitamura, K., Kawada, H., Matsumoto, Y., Kitade, T., Ishida, H., Nagata, C., 2008. Preparation and characterization of a new lipid nano-emulsion containing two cosurfactants, sodium palmitate for droplet size reduction and sucrose palmitate for stability enhancement. *Chem. Pharm. Bull.* 56, 1097–1102.
- Tang, Y.-Z., Liu, Z.-Q., 2008. Chemical kinetic behavior of chlorogenic acid in protecting erythrocyte and DNA against radical-induced oxidation. *J. Agric. Food. Chem.* 56, 11025–11029.
- Tang, S.Y., Manickam, S., Wei, T.K., Nashiru, B., 2012. Formulation development and optimization of a novel Cremophore EL-based nanoemulsion using ultrasound cavitation. *Ultrason. Sonochem.* 19, 330–345.
- Taslimi, P., 2020. Evaluation of in vitro inhibitory effects of some natural compounds on tyrosinase activity and molecular docking study: Antimelanogenesis potential. *J. Biochem. Mol. Toxicol.* 34, e22566.
- Taylor, A., Pawaskar, M., Taylor, S.L., Balkrishnan, R., Feldman, S. R., 2008. Prevalence of pigmentary disorders and their impact on quality of life: a prospective cohort study. *J. Cosmetic Dermatol.* 7, 164–168.
- Ting, Y., Hu, Y.T., Hu, J.Y., Chang, W.C., Huang, Q., Hsieh, S.C., 2019. Nanoemulsified adlay bran oil reduces tyrosinase activity and melanin synthesis in B16F10 cells and zebrafish. *Food Sci. Nutrition* 7, 3216–3223.
- Ullah, S., Park, Y., Ikram, M., Lee, S., Park, C., Kang, D., Yang, J., Akter, J., Yoon, S., Chun, P., 2018. Design, synthesis and anti-melanogenic effect of cinnamide derivatives. *Bioorg. Med. Chem.* 26, 5672–5681.
- Uto, T., Tung, N.H., Shoyama, Y., 2022. Hirsutanone Isolated from the Bark of *Alnus japonica* Attenuates Melanogenesis via Dual Inhibition of Tyrosinase Activity and Expression of Melanogenic Proteins. *Plants* 11, 1875.
- Vayalil, P.K., Elmets, C.A., Katiyar, S.K., 2003. RETRACTED: Treatment of green tea polyphenols in hydrophilic cream prevents UVB-induced oxidation of lipids and proteins, depletion of antioxidant enzymes and phosphorylation of MAPK proteins in SKH-1 hairless mouse skin. *Carcinogenesis* 24, 927–936.
- Wang, H.M., Chen, C.Y., Wen, Z.H., 2011. Identifying melanogenesis inhibitors from *Cinnamomum subavenium* with in vitro and in vivo screening systems by targeting the human tyrosinase. *Exp. Dermatol.* 20, 242–248.
- Warheit, D.B., Hoke, R.A., Finlay, C., Donner, E.M., Reed, K.L., Sayes, C.M., 2007. Development of a base set of toxicity tests using ultrafine TiO₂ particles as a component of nanoparticle risk management. *Toxicol. Lett.* 171, 99–110.
- Wik, J., Bansal, K.K., Assmuth, T., Rosling, A., Rosenholm, J.M., 2020. Facile methodology of nanoemulsion preparation using oily polymer for the delivery of poorly soluble drugs. *Drug Delivery Translat. Res.* 10, 1228–1240.
- Wypij, M., Jędrzejewski, T., Ostrowski, M., Trzcńska, J., Rai, M., Golińska, P., 2020. Biogenic silver nanoparticles: assessment of their cytotoxicity, genotoxicity and study of capping proteins. *Molecules* 25, 3022.
- Youdim, M.B., 2006. The path from anti Parkinson drug selegiline and rasagiline to multifunctional neuroprotective anti Alzheimer drugs ladostigil and m30. *Curr. Alzheimer Res.* 3, 541–550.
- Zheng, Z.-P., Cheng, K.-W., Chao, J., Wu, J., Wang, M., 2008. Tyrosinase inhibitors from paper mulberry (*Broussonetia papyrifera*). *Food Chem.* 106, 529–535.
- Zhu, W., Gao, J., 2008. The use of botanical extracts as topical skin-lightening agents for the improvement of skin pigmentation disorders. In: *Journal of Investigative Dermatology Symposium Proceedings*. Elsevier, pp. 20–24.